Dynamics of a Coherent Reflection on Direct-with-Earth Links between a Planetary Body and an Earth Station

Marc Sanchez Net*

ABSTRACT. — This article provides a comprehensive model to describe a single coherent reflection between a vehicle landed on a planetary body (e.g., the Moon or Mars) and a distant receiver on Earth. Equations to describe the received signal, and the relative phase and Doppler shift of the reflected electromagnetic wave, are first derived as a function of the system geometry. These equations are then specialized to the case of a lander and a rover, highlighting some of the differences between both types of vehicles. The resulting model is used to study the dynamics of the multipath channel in both the uplink and downlink directions using the null-to-null time interval as the metric of interest. To validate the model, the obtained analytical expressions are compared against empirical data collected with the Deep Space Network, the Chandrayaan-3 spacecraft, and the Intuitive Machines 1 mission.

I. Introduction

Multipath fading is a phenomenon of interest to NASA and other space agencies currently engaged in the robotic and human exploration of the lunar South Pole [1]. Using data from missions such as the Chandrayaan-3 (CH3) and Intuitive Machines 1 (IM1), the Jet Propulsion Laboratory (JPL) has measured multipath effects pervasively in links from the landed vehicles to the Deep Space Network (DSN) stations. These effects have caused significant link degradation, causing abnormally high frame error rates and a clear operational impact to both missions.

In this article, I provide a mathematical model to describe the multipath effect caused by a single coherent reflection in direct-with-Earth links between a spacecraft landed

*Communications Architectures and Research Section.

The research described in this publication was carried out by the Jet Propulsion Laboratory, California Institute of Technology, under a contract with the National Aeronautics and Space Administration.

on a planetary body and an Earth station, nominally the DSN. The goal is to understand the time evolution of the multipath effect (also termed dynamics of the channel), which I characterize using the null-to-null time interval. This interval indicates the amount of time that needs to elapse for the channel to experience two consecutive fade events (i.e., moments of null received power), and thus has implications on the design of the telecommunication system as well as mission operations. The results of the paper extend previous literature on the area of multipath at planetary distances (e.g., [2], [3]) by obtaining simple analytical expressions for the null-to-null time interval as a function of known system parameters such as the frequency band of operation or position of Earth in the local sky.

To simplify the analysis, this article makes the following assumptions:

- At the band of operation (S-, X-, K-, Ka-band), and at the integration times of interest, the electromagnetic (EM) field can be approximated as a ray and a surface that acts as a coherent (mirror-like) reflector. Therefore, the reflection can be approximated as a single ray that emanates from the transmitter and bounces off of the planetary surface, with a resulting EM field that adds coherently (in amplitude and phase) to the line-of-sight (LoS) field.
- Because we operate at high frequencies, the laws of specular reflection must be satisfied. Therefore, the reflection occurs in a region of the planetary surface where the angle of incidence is equal to the angle of reflection, and the incident and reflected waves are coplanar with the local surface normal vector. When modeling the EM wave as a geometric ray, this region is approximated as a single point of reflection, but in reality an area of extent approximately equal to the first Fresnel zone is needed for the coherent reflection to occur [4].
- The transmitted signal is circularly polarized, as is common practice in space communications. Furthermore, the transmit and receive antennas act as a perfect isolator of the cross-polarization, amplifying only the co-polarization. This allows the model to use scalar equations only, with the implicit understanding that polarization can be accounted for simply by multiplying all scalar equations by a complex polarization vector and using Jones' calculus.
- The reflection from the planetary surface can be modeled by a single parameter, known as the effective reflection coefficient $\rho \in \mathbb{C}$. The magnitude squared of this reflection coefficient relates the EM energy incident and reflected by the surface at different angles of incidence and reflection, and for the co-polarization.[1] Similarly, the phase of ρ indicates the phase offset introduced in the reflected EM wave by the interaction with the planetary surface.
- Because of the assumed two-ray model, the geometry of the reflection can be analyzed in most cases just taking into account the plane formed by the

[1] Part of the incident EM energy in the co-polarization is cross-polarized during the reflection process. This is already accounted for in the effective reflection coefficient ρ.

transmitter, point of reflection, and receiver. Therefore, most illustrations only depict that plane. Note that, in general, this does not mean that the point of reflection is co-aligned with the transmitter and receiver in azimuth. Therefore, the mathematical formulation developed in this article is general and makes no assumptions on the position of the reflection point, unless explicitly stated in the text.

The rest of this article is organized as follows: Section II, Section III, and Section IV presents the system model and derives equations for the null-to-null time interval for a lander and rover, and for different reflection geometries. Then, Section V compares the null-to-null time interval predicted by the model with measurements from the multipath channels experienced during surface operations by the CH3 and IM1 landers.

II. The System Model

Consider the general model of a coherent reflection as shown in Figure 1, where the indices 1, 2, and 3 indicate the transmitter, point of reflection, and receiver, respectively. The geometry is typical for a downlink and is provided for illustration purposes only; in other words, it is meant to be general and, as will be argued in Section IV, is also applicable to uplinks from an Earth station to a landed vehicle. The direct LoS wave from the transmitter to receiver is shown in black. It departs the transmitter at time t_1, and arrives at the receiver at time t_3.[2] Similarly, the reflected ray (shown in orange) departs at time t_1', impinges on the surface at time t_2', and is received at time t_3'.[3]

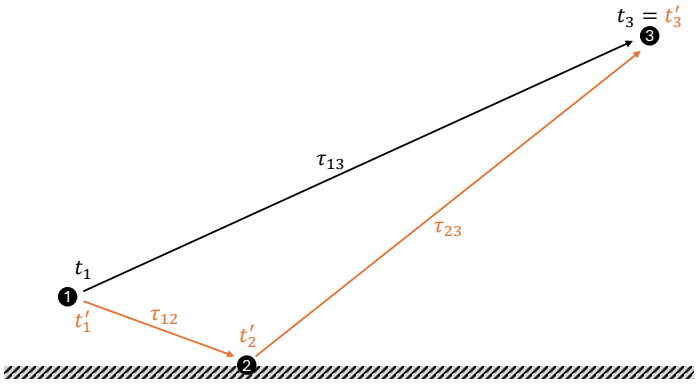

Figure 1. Model of a single coherent reflection in a downlink from a landed spacecraft to an Earth station.

[2]This article uses a classical non-relativistic model of the universe. As such, we can assume that all times expressed in a common known clock reference such as the JPL ephemeris time.

[3]In this article, quantities qualified with an apostrophe are always related to the reflected ray. To avoid confusion, time derivatives are expressed using Newton's or dot notation.

We are interested in understanding the received electric field as a function of time. Therefore, it is advantageous to set the reference time for the analysis as $t_3 = t_3'$ and note that, under this viewpoint, t_1 and t_1' represent the times at which the LoS and reflected rays departed the transmitter to arrive at the receiver at the same time. Furthermore, the times t_1, t_1', t_2', and t_3 are related by the one-way propagation delay of the EM wave, which are defined as follows:[4]

- $\tau_{13}(t_1, t_3)$ is the propagation delay of the line-of-sight ray.
- $\tau_{12}(t_1', t_2')$ is the propagation delay from the transmitter to the point of reflection.
- $\tau_{23}(t_2', t_3)$ is the propagation delay from the point of reflection to the receiver.

Define the following quantities to describe the system's state in an arbitrary reference frame:

- $\vec{\boldsymbol{r}}_1(t_1) \equiv \vec{\boldsymbol{r}}_1$ is the transmitter's position at time t_1.
- $\vec{\boldsymbol{v}}_1(t_1) \equiv \vec{\boldsymbol{v}}_1$ is the transmitter's velocity at time t_1.
- $\vec{\boldsymbol{r}}_1(t_1') \equiv \vec{\boldsymbol{r}}_1'$ is the transmitter's position at time t_1'.
- $\vec{\boldsymbol{v}}_1(t_1') \equiv \vec{\boldsymbol{v}}_1'$ is the transmitter's velocity at time t_1'.
- $\vec{\boldsymbol{r}}_2(t_2') \equiv \vec{\boldsymbol{r}}_2'$ is the position of the point of reflection at time t_2'.
- $\vec{\boldsymbol{v}}_2(t_2') \equiv \vec{\boldsymbol{v}}_2'$ is the velocity of the point of reflection at time t_2'.[5]
- $\vec{\boldsymbol{r}}_3(t_3 = t_3') \equiv \vec{\boldsymbol{r}}_3$ is the receiver's position at time t_3.
- $\vec{\boldsymbol{v}}_3(t_3 = t_3') \equiv \vec{\boldsymbol{v}}_3$ is the receiver's velocity at time t_3.
- $\vec{\boldsymbol{r}}_{13}(t_1, t_3) = \vec{\boldsymbol{r}}_3(t_3) - \vec{\boldsymbol{r}}_1(t_1) \equiv \vec{\boldsymbol{r}}_{13}$.
- $\vec{\boldsymbol{v}}_{13}(t_1, t_3) = \vec{\boldsymbol{v}}_3(t_3) - \vec{\boldsymbol{v}}_1(t_1) \equiv \vec{\boldsymbol{v}}_{13}$.
- $\vec{\boldsymbol{r}}_{12}(t_1', t_2') = \vec{\boldsymbol{r}}_2(t_2') - \vec{\boldsymbol{r}}_1(t_1') \equiv \vec{\boldsymbol{r}}_{12}'$.
- $\vec{\boldsymbol{v}}_{12}(t_1', t_2') = \vec{\boldsymbol{v}}_2(t_2') - \vec{\boldsymbol{v}}_1(t_1') \equiv \vec{\boldsymbol{v}}_{12}'$.
- $\vec{\boldsymbol{r}}_{23}(t_2', t_3) = \vec{\boldsymbol{r}}_3(t_3) - \vec{\boldsymbol{r}}_2(t_2') \equiv \vec{\boldsymbol{r}}_{23}'$.

---

[4] While τ_{ij} are indexed with two time variables (i.e., two degrees of freedom), in reality this is just a mathematical convenience for the analysis in subsequent sections. Indeed, the time of arrival of the EM wave at the receiver is necessarily constrained by the orbital motion of the spacecraft or bodies involved in the wave propagation. This orbital motion acts as a constraint in the system, eliminating one of the degrees of freedom.

[5] In general, the state of all elements in the system could by expressed in an inertial reference frame such as the J2000 reference frame. In that case, the surface of the planetary body would have a non-zero velocity.

- $\vec{\boldsymbol{v}}_{23}(t_2', t_3) = \vec{\boldsymbol{v}}_3(t_3) - \vec{\boldsymbol{v}}_2(t_2') \equiv \vec{\boldsymbol{v}}_{23}'$.

Then, under the assumption of free space propagation, the delays relating the times t_1, t_1', t_2', and t_3 are simply equal to:

$$\tau_{13}(t_1, t_3) = \frac{r_{13}}{c} \equiv \tau_{13} \tag{1}$$

$$\tau_{12}(t_1', t_2') = \frac{r_{12}'}{c} \equiv \tau_{12} \tag{2}$$

$$\tau_{23}(t_2', t_3) = \frac{r_{23}'}{c} \equiv \tau_{23}, \tag{3}$$

with c equal to the speed of light in the vacuum, and with the convention that $|\vec{\boldsymbol{a}}| = a$ denotes the magnitude of an arbitrary vector.

A. Received Signal

The received signal is the coherent sum of the LoS and reflected rays. Mathematically,[6]

$$\tilde{s}(t_3) = \tilde{s}_{13}(t_3) + \tilde{s}_{13}'(t_3), \tag{4}$$

where $\tilde{s}(t)$ is the complex baseband domain representation of the transmitted signal, $\tilde{s}_{13}(t)$ is the signal traveling on the LoS ray, and $\tilde{s}_{13}'(t)$ is the signal traveling on the reflected ray.

To characterize the channel behavior, assume the transmitter sends a narrowband signal phase modulated onto the carrier frequency.[7] Let $\phi(t)$ and $\phi'(t)$ denote the phase of the signals traveling through the LoS and reflected rays, respectively. Then,

$$\tilde{s}(t_3) = \sqrt{P}\left[e^{j\phi(t_3)} + \rho e^{j\phi'(t_3)}\right] = \sqrt{P}e^{j\phi(t_3)}\left[1 + \rho e^{j\Delta\phi(t_3)}\right] \tag{5}$$

where P denotes the total received power from the LoS ray, ρ is the effective reflection coefficient in the polarization of interest, and

$$\Delta\phi(t_3) = \phi'(t_3) - \phi(t_3) \tag{6}$$

is the phase difference between the LoS and reflected EM wave, caused by the additional distance traveled by the reflected ray while propagating toward the receiver. This phase difference causes power fluctuations at the receiver, given by

$$\begin{aligned} P_r(t_3) =& |\tilde{s}(t_3)|^2 = P|1 + \rho e^{j\Delta\phi(t_3)}|^2 \\ =& P\left[1 + |\rho|^2 + 2\left(\mathfrak{Re}\{\rho\}\cos\Delta\phi(t_3) - \mathfrak{Im}\{\rho\}\sin\Delta\phi(t_3)\right)\right] \end{aligned} \tag{7}$$

---

[6] The presence of additive white Gaussian noise (AWGN) is implicitly assumed throughout the paper, but not explicitly stated in the equations to ease notation.

[7] It follows that this characterization is not totally representative of wideband signals where intersymbol-interference (ISI) effects may be experienced.

As an example, Figure 2 plots the received power as a function of $\Delta\phi(t_3)$ and the surface reflectivity, which is assumed to be nonconductive to simplify the analysis. Note that when the LoS and reflected rays are in-phase (i.e., $\Delta\phi(t_3) = 0°$) the channel experiences a net gain, whereas when they are out of phase ($\Delta\phi(t_3) = \pm 180°$) there is a fade event with intensity that depends on the surface reflectivity. Note also that the analysis and plot have been conducted under the assumption that the LoS and reflected ray experience the same transmit plus receive gain. If that is not the case, the depth of the fades increases or decreases, but their dependence on $\Delta\phi(t_3)$ (and hence their dynamics) are not affected.

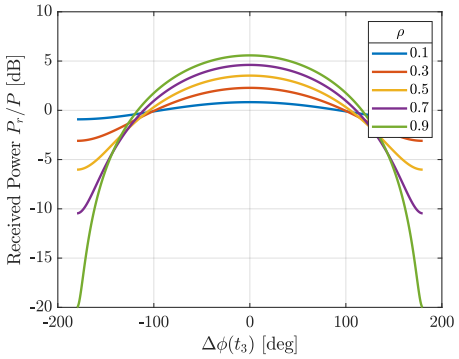

Figure 2. Normalized received power as a function of the relative phase between the LoS and reflected EM waves.

B. Phase Difference

To relate $\Delta\phi(t_3)$ to geometrical quantities of the system, we proceed in two steps: First, we note the following phase relationships:

$$\phi(t_3) = \phi(t_1) \tag{8}$$

$$\phi'(t_3) = \phi(t_1') \tag{9}$$

The first relationship simply states that the phase of the LoS ray received at time t_3 must be equal to the phase that departed from the transmitter at time t_1, with t_1 and t_3 related by the propagation delay of the LoS ray. Similarly, the second relationship states that the phase of the reflected ray at time t_3 must be equal to the phase of the ray departing from the transmitter at time t_1' (after all, the reflected ray carries a delayed copy of the transmitted signal), where t_1' accounts for the extra delay associated with the longer distance traveled by the reflected ray.

Next, we assume that for the purposes of this analysis the narrowband transmitted signal can be approximated by an unmodulated tone at constant carrier frequency f_c.

Then, the phase of the transmitted signal is simply equal to[8]

$$\phi(t) = 2\pi f_c t, \tag{10}$$

which together with Equations (8) and (9) yields

$$\Delta\phi(t_3) = \phi(t_1') - \phi(t_1) = 2\pi f_c \left(t_1' - t_1\right). \tag{11}$$

This can be expressed in terms of the propagation delays by noting that

$$t_1 = t_3 - \tau_{13} \tag{12}$$

$$t_1' = t_3 - \tau_{13}' = t_3 - (\tau_{12} + \tau_{23}) \tag{13}$$

so that

$$\Delta\phi(t_3) = 2\pi f_c \Delta\tau_{13} \tag{14}$$

with

$$\Delta\tau_{13} = \tau_{13} - \tau_{13}'. \tag{15}$$

Equations (14) and (15) simply state that the phase difference between the LoS and reflected rays is proportional to the carrier frequency and to the delta in propagation delay between the direct LoS and reflected rays.

Further simplifications are possible if we assume propagation in free space and that the receiver is far away from the transmitter and the point of reflection, as is typical in planetary scenarios.[9] In this case,

$$\begin{aligned}
\Delta\tau_{13} =& \frac{1}{c}\left[r_{13} - (r_{12}' + r_{23}')\right] \\
\approx& \frac{1}{c}\left[(r_3(t_3) - \vec{\boldsymbol{r}}_1(t_1)\cdot\hat{\boldsymbol{r}}_3(t_3)) - r_{12}' - (r_3(t_3) - \vec{\boldsymbol{r}}_2(t_2')\cdot\hat{\boldsymbol{r}}_3(t_3))\right] \\
=& \frac{1}{c}\left[\hat{\boldsymbol{r}}_3(t_3)\cdot(\vec{\boldsymbol{r}}_2(t_2') - \vec{\boldsymbol{r}}_1(t_1)) - r_{12}'\right]
\end{aligned} \tag{16}$$

where the second equality is simply the far-field approximation when $r_3 \gg r_1, r_2$. Next, I note that the deltas in time $|t_1 - t_1'|$ and $|t_1 - t_2'|$ are small, on the order of a nanosecond to a few milliseconds, so that

$$\vec{\boldsymbol{r}}_i(t_1') \approx \vec{\boldsymbol{r}}_i(t_1) \quad i \in [1,2] \tag{17}$$

$$\vec{\boldsymbol{r}}_i(t_2') \approx \vec{\boldsymbol{r}}_i(t_1) \quad i \in [1,2]. \tag{18}$$

Therefore, a good approximation to $\Delta\phi(t_3)$ can be obtained by evaluating the position of the transmitter, reflection point, and receiver at times t_1 and t_3, yielding

$$\Delta\phi(t_3) \approx \frac{2\pi}{\lambda} r_{12}(t_1)\left[\hat{\boldsymbol{r}}_3(t_3)\cdot\hat{\boldsymbol{r}}_{12}(t_1) - 1\right], \tag{19}$$

---

[8] Without loss of generality, we have assumed that at time $t = 0$ the phase is equal to 0 radians.

[9] As an example, a vehicle on the lunar South Pole communicating with a DSN station may experience a reflection a few kilometers away for the spacecraft. This distance is several orders of magnitude smaller than the ∼385,000 km that separate the Moon and Earth.

where $\vec{\boldsymbol{r}}_{12}(t) = \vec{\boldsymbol{r}}_2(t) - \vec{\boldsymbol{r}}_1(t)$. This expression has two advantages: First, it only depends on t_1 and t_3, which are easily computable with orbital simulation software such as SPICE, which automatically performs aberration corrections due to long propagation distances between planets. Second, all quantities in the equation have clear physical meaning: At any point in time, the phase offset between the LoS and reflected rays is proportional to the wave number $k = \frac{2\pi}{\lambda}$ and the extra distance traveled by the reflected wave ΔL, which, as shown in Figure 3, is given by the distance to the point of reflection minus a correction factor:

$$\Delta L = r_{12} - r_{12}\cos\varphi = r_{12}\left[1 - \hat{\boldsymbol{r}}_3 \cdot \hat{\boldsymbol{r}}_{12}\right]. \tag{20}$$

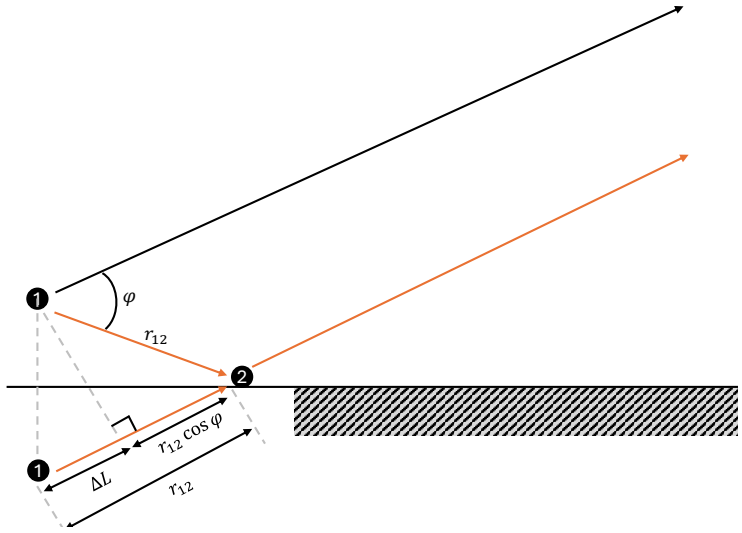

Figure 3. Additional length traveled by the reflected ray. Point 1 below the surface represents the mirror image of the transmitter. The LoS and reflected rays are parallel to each other, as required by the far-field approximation from Equation 16.

C. Differential Doppler Shift

To understand the dynamics of the received signal, it is necessary to understand the behavior of the derivative of relative phase between the LoS and reflected rays, which is proportional to the differential Doppler shift. Therefore, we seek expressions for $\frac{\partial}{\partial t_3}\Delta\phi(t_3)$.

To start, assume that the transmitter sends a perfect tone at a constant carrier frequency f_c that does not vary over time. In that case,

$$\frac{\partial}{\partial t_3}\Delta\phi(t_3) = 2\pi f_c \frac{\partial}{\partial t_3}\Delta\tau_{13} \tag{21}$$

and[10]

$$\begin{aligned}\frac{\partial}{\partial t_3}\Delta\tau_{13} =&\frac{\partial}{\partial t_3}\left\{\tau_{13}(t_1,t_3)-\tau_{12}(t_1',t_2')-\tau_{23}(t_2',t_3)\right\}\\ =&\left(\partial_{t_1}\tau_{13}\frac{dt_1}{dt_3}+\partial_{t_3}\tau_{13}\frac{dt_3}{dt_3}\right)-\left(\partial_{t_1'}\tau_{12}\frac{dt_1'}{dt_3}+\partial_{t_2'}\tau_{12}\frac{dt_2'}{dt_3}\right)-\left(\partial_{t_2'}\tau_{23}\frac{dt_2'}{dt_3}+\partial_{t_3}\tau_{23}\frac{dt_3}{dt_3}\right)\\ =&\left(\partial_{t_1}\tau_{13}\frac{dt_1}{dt_3}-\partial_{t_1'}\tau_{12}\frac{dt_1'}{dt_3}\right)-\partial_{t_2'}\left(\tau_{12}+\tau_{23}\right)\frac{dt_2'}{dt_3}+\partial_{t_3}\left(\tau_{13}-\tau_{23}\right).\end{aligned} \tag{22}$$

Next, I evaluate the time derivatives using implicit differentiation. For example, knowing that $t_1 = t_3 - \tau_{13}$ yields

$$\frac{dt_1}{dt_3} = 1 - \left[\partial_{t_1}\tau_{13}\frac{dt_1}{dt_3} + \partial_{t_3}\tau_{13}\frac{dt_3}{dt_3}\right], \tag{23}$$

which results in

$$\frac{dt_1}{dt_3} = \frac{1-\partial_{t_3}\tau_{13}}{1+\partial_{t_1}\tau_{13}}. \tag{24}$$

Using the same logic, and the fact that $t_2' = t_3 - \tau_{23}$, I get

$$\frac{dt_2'}{dt_3} = \frac{1-\partial_{t_3}\tau_{23}}{1+\partial_{t_2'}\tau_{23}} \tag{25}$$

and

$$\frac{dt_1'}{dt_3} = \frac{dt_1'}{dt_2'}\frac{dt_2'}{dt_3} = \frac{1-\partial_{t_2'}\tau_{12}}{1+\partial_{t_1'}\tau_{12}}\frac{1-\partial_{t_3}\tau_{23}}{1+\partial_{t_2'}\tau_{23}}. \tag{26}$$

Combining these results, a generic expression for the time derivative of the differential delay is obtained:

$$\begin{aligned}\frac{\partial}{\partial t_3}\Delta\tau_{13} =&\partial_{t_1}\tau_{13}\frac{1-\partial_{t_3}\tau_{13}}{1+\partial_{t_1}\tau_{13}} - \partial_{t_1'}\tau_{12}\frac{1-\partial_{t_2'}\tau_{12}}{1+\partial_{t_1'}\tau_{12}}\frac{1-\partial_{t_3}\tau_{23}}{1+\partial_{t_2'}\tau_{23}}\\ &-\partial_{t_2'}\left(\tau_{12}+\tau_{23}\right)\frac{1-\partial_{t_3}\tau_{23}}{1+\partial_{t_2'}\tau_{23}} + \partial_{t_3}\left(\tau_{13}-\tau_{23}\right).\end{aligned} \tag{27}$$

To proceed further, assume propagation in free space and note that the derivative of the norm of a generic vector $\vec{\boldsymbol{a}}(t)$ is equal to $\frac{d}{dt}|\vec{\boldsymbol{a}}(t)| = \hat{\boldsymbol{a}}(t)\cdot\frac{d}{dt}\vec{\boldsymbol{a}}(t)$. Hence, the following relationships result:

$$\partial_{t_1'}\tau_{12} = -\frac{1}{c}\vec{\boldsymbol{v}}_1(t_1')\cdot\hat{\boldsymbol{r}}_{12}(t_1',t_2') \equiv -\frac{1}{c}\vec{\boldsymbol{v}}_1'\cdot\hat{\boldsymbol{r}}_{12}' \tag{28}$$

$$\partial_{t_2'}\tau_{12} = +\frac{1}{c}\vec{\boldsymbol{v}}_2(t_2')\cdot\hat{\boldsymbol{r}}_{12}(t_1',t_2') \equiv +\frac{1}{c}\vec{\boldsymbol{v}}_2'\cdot\hat{\boldsymbol{r}}_{12}' \tag{29}$$

$$\partial_{t_2'}\tau_{23} = -\frac{1}{c}\vec{\boldsymbol{v}}_2(t_2')\cdot\hat{\boldsymbol{r}}_{23}(t_2',t_3) \equiv -\frac{1}{c}\vec{\boldsymbol{v}}_2'\cdot\hat{\boldsymbol{r}}_{23}' \tag{30}$$

$$\partial_{t_3}\tau_{23} = +\frac{1}{c}\vec{\boldsymbol{v}}_3(t_3)\cdot\hat{\boldsymbol{r}}_{23}(t_2',t_3) \equiv +\frac{1}{c}\vec{\boldsymbol{v}}_3\cdot\hat{\boldsymbol{r}}_{23}' \tag{31}$$

$$\partial_{t_1}\tau_{13} = -\frac{1}{c}\vec{\boldsymbol{v}}_1(t_1)\cdot\hat{\boldsymbol{r}}_{13}(t_1,t_3) \equiv -\frac{1}{c}\vec{\boldsymbol{v}}_1\cdot\hat{\boldsymbol{r}}_{13} \tag{32}$$

$$\partial_{t_3}\tau_{13} = +\frac{1}{c}\vec{\boldsymbol{v}}_3(t_3)\cdot\hat{\boldsymbol{r}}_{13}(t_1,t_3) \equiv +\frac{1}{c}\vec{\boldsymbol{v}}_3\cdot\hat{\boldsymbol{r}}_{13} \tag{33}$$

[10] To ease notation, in some cases the partial derivative $\frac{\partial}{\partial x}f(x)$ is expressed using D-notation $\partial_x f(x)$.

which, when substituted into Equation (27) result in

$$\begin{aligned}\frac{\partial}{\partial t_3}\Delta\tau_{13} = &-\frac{1}{c}\vec{\boldsymbol{v}}_1\cdot\hat{\boldsymbol{r}}_{13}\frac{c-\vec{\boldsymbol{v}}_3\cdot\hat{\boldsymbol{r}}_{13}}{c-\vec{\boldsymbol{v}}_1\cdot\hat{\boldsymbol{r}}_{13}}+\frac{1}{c}\vec{\boldsymbol{v}}_1'\cdot\hat{\boldsymbol{r}}_{12}'\frac{c-\vec{\boldsymbol{v}}_2'\cdot\hat{\boldsymbol{r}}_{12}'}{c-\vec{\boldsymbol{v}}_1'\cdot\hat{\boldsymbol{r}}_{12}'}\frac{c-\vec{\boldsymbol{v}}_3\cdot\hat{\boldsymbol{r}}_{23}'}{c-\vec{\boldsymbol{v}}_2'\cdot\hat{\boldsymbol{r}}_{23}'}\\ &-\frac{1}{c}\vec{\boldsymbol{v}}_2'\cdot\left(\hat{\boldsymbol{r}}_{12}'-\hat{\boldsymbol{r}}_{23}'\right)\frac{c-\vec{\boldsymbol{v}}_3\cdot\hat{\boldsymbol{r}}_{23}'}{c-\vec{\boldsymbol{v}}_2'\cdot\hat{\boldsymbol{r}}_{23}'}+\frac{1}{c}\vec{\boldsymbol{v}}_3\cdot\left(\hat{\boldsymbol{r}}_{13}-\hat{\boldsymbol{r}}_{23}'\right).\end{aligned} \tag{34}$$

Next, assume that the deltas in time $|t_1 - t_1'|$ and $|t_1 - t_2'|$ are small so that the position and velocity vectors evaluated at t_1' and t_2' can be well approximated by those at time t_1. This results in

$$\begin{aligned}\frac{\partial}{\partial t_3}\Delta\tau_{13} \approx &-\frac{1}{c}\vec{\boldsymbol{v}}_1\cdot\left(\hat{\boldsymbol{r}}_{13}\frac{c-\vec{\boldsymbol{v}}_3\cdot\hat{\boldsymbol{r}}_{13}}{c-\vec{\boldsymbol{v}}_1\cdot\hat{\boldsymbol{r}}_{13}}-\hat{\boldsymbol{r}}_{12}\frac{c-\vec{\boldsymbol{v}}_2\cdot\hat{\boldsymbol{r}}_{12}}{c-\vec{\boldsymbol{v}}_1\cdot\hat{\boldsymbol{r}}_{12}}\frac{c-\vec{\boldsymbol{v}}_3\cdot\hat{\boldsymbol{r}}_{23}}{c-\vec{\boldsymbol{v}}_2\cdot\hat{\boldsymbol{r}}_{23}}\right)\\ &-\frac{1}{c}\vec{\boldsymbol{v}}_2\cdot\left(\hat{\boldsymbol{r}}_{12}-\hat{\boldsymbol{r}}_{23}\right)\frac{c-\vec{\boldsymbol{v}}_3\cdot\hat{\boldsymbol{r}}_{23}}{c-\vec{\boldsymbol{v}}_2\cdot\hat{\boldsymbol{r}}_{23}}+\frac{1}{c}\vec{\boldsymbol{v}}_3\cdot\left(\hat{\boldsymbol{r}}_{13}-\hat{\boldsymbol{r}}_{23}\right),\end{aligned} \tag{35}$$

where all position and velocity vectors for the transmitter and point of reflection are evaluated at time t_1, and the state of the receiver is evaluated at time t_3.

Further approximations are possible by assuming that the speed of light c is much larger than the speed of any physical object in the system. In that case, an approximation of Equation (35) accurate up to $\mathcal{O}\left(\frac{1}{c^2}\right)$ can be obtained applying the Taylor expansion of $1/(1-x)$ when $x \to 0$ so that

$$\frac{c-\vec{\boldsymbol{v}}_j\cdot\hat{\boldsymbol{r}}_{ij}}{c-\vec{\boldsymbol{v}}_i\cdot\hat{\boldsymbol{r}}_{ij}} \approx \left[1-\frac{\vec{\boldsymbol{v}}_j\cdot\hat{\boldsymbol{r}}_{ij}}{c}\right]\left[1+\frac{\vec{\boldsymbol{v}}_i\cdot\hat{\boldsymbol{r}}_{ij}}{c}\right] \approx 1-\frac{\vec{\boldsymbol{v}}_{ij}\cdot\hat{\boldsymbol{r}}_{ij}}{c}+\mathcal{O}\left(\tfrac{1}{c^2}\right), \tag{36}$$

with $\vec{\boldsymbol{v}}_{ij} = \vec{\boldsymbol{v}}_j - \vec{\boldsymbol{v}}_i$ and $i, j \in [1, 2, 3]$. Consequently,

$$\begin{aligned}\frac{\partial}{\partial t_3}\Delta\tau_{13} \approx &\frac{\vec{\boldsymbol{v}}_{13}\cdot\hat{\boldsymbol{r}}_{13}-(\vec{\boldsymbol{v}}_{12}\cdot\hat{\boldsymbol{r}}_{12}+\vec{\boldsymbol{v}}_{23}\cdot\hat{\boldsymbol{r}}_{23})}{c}\\ &+\frac{(\vec{\boldsymbol{v}}_{13}\cdot\hat{\boldsymbol{r}}_{13})(\vec{\boldsymbol{v}}_1\cdot\hat{\boldsymbol{r}}_{13})-(\vec{\boldsymbol{v}}_{12}\cdot\hat{\boldsymbol{r}}_{12})(\vec{\boldsymbol{v}}_1\cdot\hat{\boldsymbol{r}}_{12})+(\vec{\boldsymbol{v}}_{23}\cdot\hat{\boldsymbol{r}}_{23})(\vec{\boldsymbol{v}}_{12}\cdot\hat{\boldsymbol{r}}_{12}-\vec{\boldsymbol{v}}_2\cdot\hat{\boldsymbol{r}}_{23})}{c^2}\\ &+\mathcal{O}\left(\tfrac{1}{c^3}\right).\end{aligned} \tag{37}$$

Finally, using the fact that $\vec{\boldsymbol{v}}_{ij}\cdot\hat{\boldsymbol{r}}_{ij} = \dot{r}_{ij}$ yields a compact expression

$$\frac{\partial}{\partial t_3}\Delta\tau_{13} \approx \frac{\dot{r}_{13}-(\dot{r}_{12}+\dot{r}_{23})}{c}+\frac{\dot{r}_{13}(\vec{\boldsymbol{v}}_1\cdot\hat{\boldsymbol{r}}_{13})-\dot{r}_{12}(\vec{\boldsymbol{v}}_1\cdot\hat{\boldsymbol{r}}_{12})+\dot{r}_{23}(\dot{r}_{12}-\vec{\boldsymbol{v}}_2\cdot\hat{\boldsymbol{r}}_{23})}{c^2} \tag{38}$$

from which the differential phase can be calculated using Equation (21), and the differential Doppler shift can be obtained as

$$\Delta\nu(t_3) = \frac{1}{2\pi}\frac{\partial}{\partial t_3}\Delta\phi_{13} = f_c\frac{\partial}{\partial t_3}\Delta\tau_{13}. \tag{39}$$

III. Dynamics of a Downlink with a Single Coherent Reflection

In this section we use the theoretical results from Section II to understand the dynamics of a coherent reflection in a downlink at planetary distances. To simplify the

problem, I assume that the leading term in Equation (38) provides sufficient accuracy for the analysis. In other words,

$$\Delta\nu(t_3) \approx \frac{\dot{r}_{13} - (\dot{r}_{12} + \dot{r}_{23})}{\lambda}, \tag{40}$$

which is analogous to a well-known result in the bistatic radar literature, which states that the Doppler shift of the reflected signal is equal to the rate of change of the distance from the transmitter to the reflection point ($\dot{r}_{12}$), and from the reflection point to the receiver ($\dot{r}_{23}$) [5].

Assume that all calculations are performed in a reference frame centered on the transmitter and fixed to the planetary body where the reflection is occurring so that, by definition, $\vec{\boldsymbol{r}}_1(t) = 0$ and $\vec{\boldsymbol{v}}_2(t) = 0\ \forall t$.[11] Then, the differential Doppler shift expressed in vectorial form can be rewritten as

$$\Delta\nu(t_3) \approx \frac{\vec{\boldsymbol{v}}_1 \cdot (\hat{\boldsymbol{r}}_{12} - \hat{\boldsymbol{r}}_{13}) + \vec{\boldsymbol{v}}_3 \cdot (\hat{\boldsymbol{r}}_{13} - \hat{\boldsymbol{r}}_{23})}{\lambda}. \tag{41}$$

A. Differential Doppler Shift for a Lander

In the reference frame of choice, a stationary landed vehicle satisfies $\vec{\boldsymbol{v}}_1(t) = 0\ \forall t$ by definition. Therefore,

$$\Delta\nu(t_3) \approx \frac{\vec{\boldsymbol{v}}_3 \cdot (\hat{\boldsymbol{r}}_{13} - \hat{\boldsymbol{r}}_{23})}{\lambda} \tag{42}$$

and, consequently, the system dynamics will be driven only by the motion of the receiver in the local sky (i.e., as seen by the transmitter). Furthermore, at planetary distances, it is easy to see that the direction vectors $\hat{\boldsymbol{r}}_{13}$ and $\hat{\boldsymbol{r}}_{23}$ will be almost parallel, as shown in Figure 3. Consequently, intuitively we expect the differential Doppler shift to be very small, typically less than 0.1 Hz.

Let the receiver be located at coordinates (θ_3, φ_3) as seen by the lander's transmitting antenna in the local sky (i.e., with respect to a topocentric reference frame centered on the antenna) and expressed in spherical coordinates, with θ equal to the receiver's colatitude position (i.e., the angle measured from the zenith direction of the lander's topocentric frame) and φ equal to the azimuth angle measured from the north direction in the local XY plane. Assume also that the same receiver is located at coordinates $(\theta_3 + \varepsilon_1, \varphi_3 + \varepsilon_2)$ as seen by the point of reflection so that

$$\begin{aligned} \hat{\boldsymbol{r}}_{13} - \hat{\boldsymbol{r}}_{23} = &\left[\sin\theta_3 \cos\varphi_3 - \sin(\theta_3 + \varepsilon_1)\cos(\varphi_3 + \varepsilon_2)\right] \hat{\boldsymbol{x}} \\ &+ \left[\sin\theta_3 \sin\varphi_3 - \sin(\theta_3 + \varepsilon_1)\sin(\varphi_3 + \varepsilon_2)\right] \hat{\boldsymbol{y}} \\ &+ \left[\cos\theta_3 - \cos(\theta_3 + \varepsilon_1)\right] \hat{\boldsymbol{z}}. \end{aligned} \tag{43}$$

[11] Body-fixed frames are non-inertial and thus require relativistic treatment of the Doppler shift to be accurate. However, because the model developed in Section II is non-relativistic, this article ignores this fact.

Because the distance to the point of reflection is much smaller than the distance from transmitter to receiver, we may assume that $\varepsilon_1 \ll 1$ and $\varepsilon_2 \ll 1$. Therefore, upon using basic trigonometric identities and the small-angle approximation for sine and cosine, I get

$$\begin{aligned}\hat{\boldsymbol{r}}_{13} - \hat{\boldsymbol{r}}_{23} \approx &\left[-\varepsilon_1 \cos\theta_3 \cos\varphi_3 + \varepsilon_2 \sin\theta_3 \sin\varphi_3\right] \hat{\boldsymbol{x}} \\ &+ \left[-\varepsilon_1 \cos\theta_3 \sin\varphi_3 - \varepsilon_2 \sin\theta_3 \cos\varphi_3\right] \hat{\boldsymbol{y}} \\ &+ \left[\varepsilon_1 \sin\theta_3\right] \hat{\boldsymbol{z}}.\end{aligned} \tag{44}$$

From this approximated value, we note the following properties:

$$|\hat{\boldsymbol{r}}_{13} - \hat{\boldsymbol{r}}_{23}| = \sqrt{(\hat{\boldsymbol{r}}_{13} - \hat{\boldsymbol{r}}_{23}) \cdot (\hat{\boldsymbol{r}}_{13} - \hat{\boldsymbol{r}}_{23})} = \sqrt{\varepsilon_1^2 + \varepsilon_2^2 \sin^2\theta_3} \tag{45}$$

$$\hat{\boldsymbol{r}}_{13} \cdot (\hat{\boldsymbol{r}}_{13} - \hat{\boldsymbol{r}}_{23}) = 0. \tag{46}$$

Equation (46) has an important physical meaning: It shows that whereas the Doppler shift of an electromagnetic signal is proportional to the radial speed between transmitter and receiver, the *differential* Doppler shift at planetary distances is independent from it. In other words, $\Delta\nu$ does not depend on $\dot{r}$, it depends on $\dot{\theta}$ and $\dot{\varphi}$, the angular speeds of the receiver in the transmitter's local sky.

To formalize this relationship, let the receiver's velocity vector be expressed in spherical coordinates as

$$\vec{\boldsymbol{v}}_3(t_3) = \dot{r}_3 \hat{\boldsymbol{r}} + r_3 \dot{\theta}_3 \hat{\boldsymbol{\theta}} + r_3 \sin\theta_3 \dot{\varphi}_3 \hat{\boldsymbol{\varphi}}, \tag{47}$$

where both $\dot{\theta}_3$ and $\dot{\varphi}_3$ are expressed in radians per second, the vectors $\hat{\boldsymbol{r}}$, $\hat{\boldsymbol{\theta}}$, and $\hat{\boldsymbol{\varphi}}$ are the spherical coordinate basis in the receiver's direction,

$$\hat{\boldsymbol{r}} = \sin\theta_3 \cos\varphi_3 \hat{\boldsymbol{x}} + \sin\theta_3 \sin\varphi_3 \hat{\boldsymbol{y}} + \cos\theta_3 \hat{\boldsymbol{z}} \tag{48}$$

$$\hat{\boldsymbol{\theta}} = \cos\theta_3 \cos\varphi_3 \hat{\boldsymbol{x}} + \cos\theta_3 \sin\varphi_3 \hat{\boldsymbol{y}} - \sin\theta_3 \hat{\boldsymbol{z}} \tag{49}$$

$$\hat{\boldsymbol{\varphi}} = -\sin\varphi_3 \hat{\boldsymbol{x}} + \cos\varphi_3 \hat{\boldsymbol{y}} \tag{50}$$

and the dependence of all terms in the right-hand side of these equations with t_3 is assumed (including the basis vectors) but not explicitly shown to ease notation. This velocity can be expressed in Cartesian coordinates by applying the Jacobian transformation matrix from spherical to rectangular coordinates, which results in

$$\begin{aligned}\vec{\boldsymbol{v}}_3 = &\left[\sin\theta_3 \cos\varphi_3 \dot{r}_3 + r_3 \cos\theta_3 \cos\varphi_3 \dot{\theta}_3 - r_3 \sin\theta_3 \sin\varphi_3 \dot{\varphi}_3\right] \hat{\boldsymbol{x}} \\ &+ \left[\sin\theta_3 \sin\varphi_3 \dot{r}_3 + r_3 \cos\theta_3 \sin\varphi_3 \dot{\theta}_3 - r_3 \sin\theta_3 \cos\varphi_3 \dot{\varphi}_3\right] \hat{\boldsymbol{y}} \\ &+ \left[\cos\theta_3 \dot{r}_3 - r_3 \sin\theta_3 \dot{\theta}_3\right] \hat{\boldsymbol{z}}.\end{aligned} \tag{51}$$

Equations (44) and (51) can now be combined to show that

$$\vec{\boldsymbol{v}}_3 \cdot (\hat{\boldsymbol{r}}_{13} - \hat{\boldsymbol{r}}_{23}) \approx -r_3 \left[\varepsilon_1 \dot{\theta}_3 + \varepsilon_2 \sin^2\theta_3 \dot{\varphi}_3\right], \tag{52}$$

which follows simply by carrying out the dot product multiplication and collecting terms using basic trigonometric identities.

Next, we consider how the angles ε_1 and ε_2 depend with the distance r_3. To facilitate the discussion, Figure 4 shows the geometry of an arbitrary reflection projected onto the plane containing the $\hat{\boldsymbol{\theta}}$ vector (side view) and the XY plane (top view). Consider first Figure 4a and note that, from triangle $\widehat{234}$,

$$\tan\varepsilon_1 = \frac{L_\theta \sin\theta_{23}}{r_{13} - L_\theta \cos\theta_{23}}, \tag{53}$$

where $\theta_{23} = -(\theta_3 - \theta_2)$ is the difference in colatitude between the ray toward the receiver (θ_3) and the reflection point (θ_2), with positive sign, and L_θ is the magnitude of $\vec{\boldsymbol{r}}_{12}$ projected onto the plane containing $\hat{\boldsymbol{\theta}}$:

$$L_\theta = |\vec{\boldsymbol{r}}_{12} - (\vec{\boldsymbol{r}}_{12}\cdot\hat{\boldsymbol{\varphi}})\hat{\boldsymbol{\varphi}}| = \sqrt{r_{12}^2 - (\vec{\boldsymbol{r}}_{12}\cdot\hat{\boldsymbol{\varphi}})^2} = r_{12}\sqrt{1-(\hat{\boldsymbol{r}}_{12}\cdot\hat{\boldsymbol{\varphi}})^2} = r_{12}\sin\Phi_{12} \tag{54}$$

with Φ_{12} equal to the angle between $\hat{\boldsymbol{r}}_{12}$ and $\hat{\boldsymbol{\varphi}}$.

Assuming that $L_\theta \ll r_{13}$, as is always the case at planetary distances, Equation (53) can be approximated as follows:

$$\tan\varepsilon_1 = \frac{L_\theta \sin\theta_{23}}{r_{13} - L_\theta \cos\theta_{23}} \approx \frac{L_\theta}{r_{13}}\sin\theta_{23} \approx \varepsilon_1 \tag{55}$$

where the last step follows from the small-angle approximation of the tangent. The exact same reasoning can be used in Figure 4b for the XY plane, which leads to

$$\tan\varepsilon_2 = \frac{L_\varphi \sin\varphi_{23}}{r_{13} - L_\varphi \cos\varphi_{23}} \approx \frac{L_\varphi}{r_{13}}\sin\varphi_{23} \approx \varepsilon_2 \tag{56}$$

with $\varphi_{23} = |\varphi_3 - \varphi_2|$ and

$$L_\varphi = |\vec{\boldsymbol{r}}_{12} - (\vec{\boldsymbol{r}}_{12}\cdot\hat{\boldsymbol{z}})\hat{\boldsymbol{z}}| = \sqrt{r_{12}^2 - (\vec{\boldsymbol{r}}_{12}\cdot\hat{\boldsymbol{z}})^2} = r_{12}\sqrt{1-(\hat{\boldsymbol{r}}_{12}\cdot\hat{\boldsymbol{z}})^2} = r_{12}\sin\Theta_{12}, \tag{57}$$

where Θ_{12} is the angle between $\hat{\boldsymbol{r}}_{12}$ and $\hat{\boldsymbol{z}}$.[12]

Combining these results with Equation (52), and noting that $\vec{\boldsymbol{r}}_{13} = \vec{\boldsymbol{r}}_3$ in the assumed frame of reference, yields[13]

$$\vec{\boldsymbol{v}}_3 \cdot (\hat{\boldsymbol{r}}_{13} - \hat{\boldsymbol{r}}_{23}) \approx -r_{12}\left[w_\theta \dot{\theta}_3 + w_\varphi \dot{\varphi}_3\right] \tag{58}$$

with

$$w_\theta = \sin\Phi_{12}\sin\theta_{23} \tag{59}$$

$$w_\varphi = \sin\Theta_{12}\sin\varphi_{23}\sin^2\theta_3 \tag{60}$$

representing weight factors that capture the relative importance of the receiver's angular speed in the azimuthal and colatitude directions. These expressions can be

[12] Recall here that the azimuth angle φ is defined in the XY plane of the transmitting antenna's topocentric frame. Therefore, the unitary vector perpendicular to the plane where azimuth is defined is $\hat{\boldsymbol{z}}$.

[13] To ease notation, all terms on the right hand side of this equation depend with time even if their time dependence is not explicitly stated.

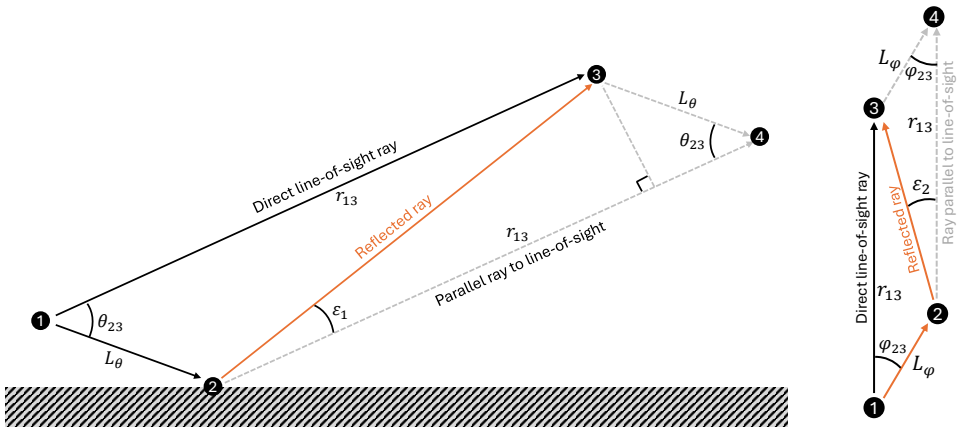

(a) Side view. **(b) Top view.**

Figure 4. Illustration of ε_1 and ε_2 angles for an arbitrary reflection. Figure 4a shows the system geometry projected onto the plane containing the vector $\hat{\theta}$. Figure 4b shows the projection onto the XY plane. Points 1, 2, and 3 indicate transmitter, point of reflection, and receiver, respectively. Point 4 is the "fictitious" position where the receiver would be if the reflected ray departing from 2 was perfectly parallel to the direct line-of-sight ray.

converted to azimuth and elevation in the transmitter's topocentric frame simply by noting that elevation ϵ is defined as

$$\epsilon = 90 - \theta \tag{61}$$

$$\dot{\epsilon} = -\dot{\theta} \tag{62}$$

and $\epsilon_{23} = \epsilon_3 - \epsilon_2 = -\theta_{23}$, so that

$$\vec{\boldsymbol{v}}_3 \cdot (\hat{\boldsymbol{r}}_{13} - \hat{\boldsymbol{r}}_{23}) \approx -\, r_{12}\left[w_\epsilon \dot{\epsilon}_3 + w_\varphi \dot{\varphi}_3\right] \tag{63}$$

$$w_\epsilon = \sin\Phi_{12} \sin\epsilon_{23} \tag{64}$$

$$w_\varphi = \sin\Theta_{12} \sin\varphi_{23} \cos^2\epsilon_3. \tag{65}$$

Using this result, I obtain the final expression for the differential Doppler shift as

$$\Delta\nu(t_3) \approx -\frac{r_{12}}{\lambda}\left[w_\epsilon \dot{\epsilon}_3 + w_\varphi \dot{\varphi}_3\right] \tag{66}$$

with w_ϵ and w_φ given by Equations (64) and (65), respectively. It states that the time dynamics of a coherent (mostly specular) reflection in a link from a spacecraft in a planetary body to an Earth station (or distant orbiting spacecraft) is driven by:

- The carrier frequency, with higher frequencies experiencing more frequent fades;
- The distance to the point of reflection on the planetary surface, with farther away reflections experiencing more frequent fades; and
- The angular velocity of the receiver in the transmitter's local sky, with most of the contribution coming from changes in elevation rather than azimuth.

Furthermore, if the reflection point is located in the plane containing the LoS ray, as is most common, then $\Phi_{12} = 90$ deg and $\varphi_{23} = 0$ deg so that only $\dot{\epsilon}$ contributes to the differential Doppler shift:

$$\Delta\nu(t_3) \approx -\frac{r_{12}}{\lambda}\dot{\epsilon}_3 \sin\epsilon_{23}. \tag{67}$$

B. Null-to-Null Time Interval for a Lander

I now study the amount of time that needs to elapse for the direct-to-Earth (DTE) link to experience two consecutive fades, which I call null-to-null time interval and denote as T_{null}.

Assume that at time t_0 the DTE link is experiencing a deep fade because the LoS and reflected EM waves arrive at the receiver out of phase. Mathematically, this simply states that $\Delta\phi(t_0) = \pi$ (or any positive or negative odd multiple of π). Then, T_{null} can be calculated as the amount of time that needs to elapse for $\Delta\phi$ to advance or be delayed by 2π radians. In other words, $\Delta\phi(t_0 + T_{\text{null}}) = \Delta\phi(t_0) \pm 2\pi$ which, after rearranging the terms, results in

$$\Delta\phi(t_0 + T_{\text{null}}) - \Delta\phi(t_0) = \pm 2\pi. \tag{68}$$

I can now invoke the fundamental theorem of calculus on the left-hand side of Equation (68) to state that

$$\int_{t_0}^{t_0+T_{\text{null}}} \Delta\dot{\phi}(t)dt = \pm 2\pi. \tag{69}$$

Furthermore, I can also use the fact that, by definition, $\Delta\dot{\phi}(t) = 2\pi\Delta\nu(t)$ to obtain

$$\int_{t_0}^{t_0+T_{\text{null}}} \Delta\nu(t)dt = \pm 1, \tag{70}$$

where $\Delta\nu(t)$ is the differential Doppler shift given by the results derived in the previous section. Note that if the position of the reflection point is known, then T_{null} is the only variable in Equation (70), so we can solve for it either analytically or via numerical integration.

For example, in general,[14]

$$\int_{t_0}^{t_0+T_{\text{null}}} \frac{r_{12}(t)}{\lambda}\left[w_\epsilon(t)\dot{\epsilon}(t) + w_\varphi(t)\dot{\varphi}(t)\right]dt = \pm 1 \tag{71}$$

[14] In Section III.A the time of analysis is denoted t_3, which is equal to time of arrival of the signal and reflected rays at the receiver. To ease notation in this section, we use the symbol t instead to express the same quantity.

where the dependence of all parameters with time has been made explicit. At planetary distances, and for a short time window lasting T_{null} seconds, we may assume that the receiver's angular speed in the local sky is well approximated by a linear Taylor expansion:

$$\epsilon(t) \approx \dot{\epsilon}_0(t - t_0) + \epsilon_0 \tag{72}$$

$$\varphi(t) \approx \dot{\varphi}_0(t - t_0) + \varphi_0, \tag{73}$$

where $\dot{\epsilon}_0$ and $\dot{\varphi}_0$ are real numbers, constant in time, and equal to the angular speeds of the receiver at time t_0.[15] Therefore, Equation (71) simplifies to

$$\int_{t_0}^{t_0+T_{\text{null}}} \frac{r_{12}(t)}{\lambda} \left[w_\epsilon(t)\dot{\epsilon}_0 + w_\varphi(t)\dot{\varphi}_0 \right] dt \approx \pm 1 \tag{74}$$

Further approximations for T_{null} are only possibly after making assumptions about the reflection point location. As an example, consider a DTE link from a lunar lander located close to the Moon's South Pole and assume the two reflection mechanisms shown in Figure 5. Assume also that $w_\varphi \approx 0$ because the Moon is tidal-locked with Earth (i.e., the azimuthal movement of a ground station in the lunar sky is small) and the reflection is specular (hence Figure 5 depicts the specular reflection plane).

In Figure 5a a specular reflection is occurring right in front of the lander. Comparing this geometry with the system model from Sections II and III.A, it is apparent that

$$r_{12} = \frac{h}{\sin \epsilon} \tag{75}$$

$$\epsilon_{23} = 2\epsilon \tag{76}$$

$$\Phi_{12} = 90^\circ. \tag{77}$$

Therefore, applying these facts to Equation (74) results in

$$\int_{t_0}^{t_0+T_{\text{null}}} \frac{h}{\sin \epsilon(t)} \sin(2\epsilon(t)) dt \approx \pm \frac{\lambda}{\dot{\epsilon}_0}, \tag{78}$$

which can be simplified by using the trigonometric identity $\sin(2x) = 2 \sin x \cos x$ to yield

$$\int_{t_0}^{t_0+T_{\text{null}}} \cos \epsilon(t) dt \approx \pm \frac{\lambda/h}{2\dot{\epsilon}_0}. \tag{79}$$

The integral of the left-hand side of this equation can be solved analytically when $\epsilon(t)$ is approximated using Equation (72) and constrained to $\epsilon(t) \in [0^\circ, 90^\circ]$

---

[15] In Section III.A the angular speed of the receiver is denoted $\dot{\epsilon}(t)$ and $\dot{\varphi}(t)$. They are general functions of time, but the time dependence is not explicitly indicted to ease notation. In this section, I am assuming that for T_{null} seconds $\dot{\epsilon}(t) \approx \dot{\epsilon}_0$ and $\dot{\varphi}(t) \approx \dot{\varphi}_0$.

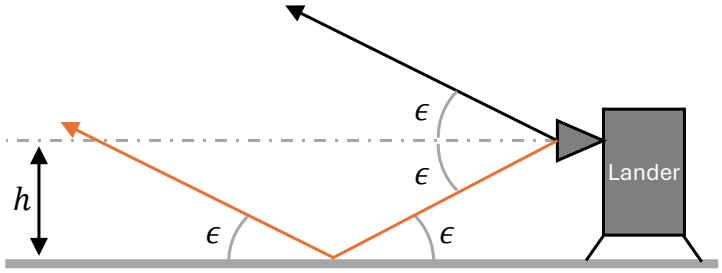

(a) Reflection occurring right in front of the lander.

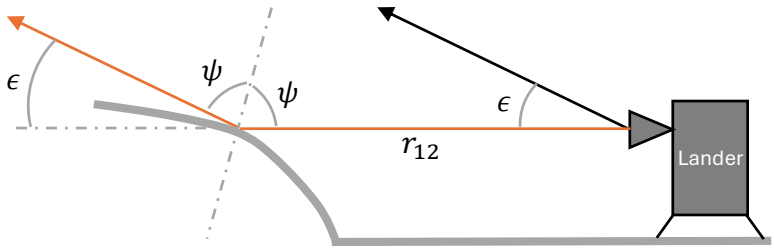

(b) Reflection occurring at a distance, in a the slope of a hill or obstacle that is properly oriented for the conditions of specular reflection to be satisfied.

Figure 5. Illustration of two possible reflection mechanisms for a lunar lander communicating with an Earth station (not shown). The angle ϵ is the elevation angle.

$\forall t \in [t_0, t_0 + T_{\text{null}}]$ resulting in

$$\int_{t_0}^{t_0+T_{\text{null}}} \cos\epsilon(t)dt = \frac{\sin(\dot{\epsilon}_0 T_{\text{null}} + \epsilon_0) - \sin\epsilon_0}{\dot{\epsilon}_0} \approx T_{\text{null}} \cos\epsilon_0, \tag{80}$$

where the second equality follows from the fact that Earth never rises to more than ∼10 to ∼15 degrees above the horizon when seen from a lunar lander located close to the lunar South Pole and, hence, the small angle approximation for the sine function can be invoked. Therefore, this result can be combined with Equation (79) to obtain the final expression

$$T_{\text{null}} \approx \frac{\lambda/(2h)}{|\dot{\epsilon}_0| \cos\epsilon_0} \tag{81}$$

where the absolute value has been used to ensure T_{null} is greater than zero.

A similar reasoning can be applied to the reflection mechanism shown in Figure 5b. In this case,

$$r_{12} = L \tag{82}$$

$$\epsilon_{23} = \epsilon \tag{83}$$

$$\Phi_{12} = 90°, \tag{84}$$

where L is the distance to the reflection point and it is assumed to be large enough (e.g., kilometers) so that it is approximately constant in the interval T_{null}. Therefore, using Equation (74) I get

$$\int_{t_0}^{t_0+T_{\text{null}}} \sin\epsilon(t)dt \approx \pm\frac{\lambda/L}{\dot{\epsilon}_0}. \tag{85}$$

The integral on the left-hand side can be solved using Equation (72) as follows:

$$\begin{aligned}\int_{t_0}^{t_0+T_{\text{null}}} \sin\epsilon(t)dt =& \frac{1}{\dot{\epsilon}_0}\left[\cos\epsilon_0 - \cos(\dot{\epsilon}_0 T_{\text{null}} + \epsilon_0)\right] \\ =& \frac{2}{\dot{\epsilon}_0}\sin\left(\frac{1}{2}\dot{\epsilon}_0 T_{\text{null}} + \epsilon_0\right)\sin\left(\frac{\dot{\epsilon}_0 T_{\text{null}}}{2}\right) \\ \approx& \frac{2}{\dot{\epsilon}_0}\sin\epsilon_0\frac{\dot{\epsilon}_0 T_{\text{null}}}{2} = T_{\text{null}}\sin\epsilon_0,\end{aligned} \tag{86}$$

where the first equality follows from a trigonometric identity, and the approximation follows from the fact that $\frac{1}{2}\dot{\epsilon}_0 T_{\text{null}} \ll \epsilon_0$ and the small angle approximation for the sine.[16] Combining this result with the right-hand side of Equation (85) provides a new expression for the null-to-null time applicable to the reflection mechanism of Figure 5b:

$$T_{\text{null}} \approx \frac{\lambda/L}{|\dot{\epsilon}_0|\sin\epsilon_0}. \tag{87}$$

C. Differential Doppler Shift for a Rover

Let us now consider a rover on the surface of a planetary body. Assume that its mobility system has a maximum instantaneous speed of $v_{\max}$ meters per second, and that the direction of motion is arbitrary and constrained only by the local terrain slopes (i.e., the rover wheels must always touch the ground). Then, from Equation (41) it is clear that the differential Doppler shift and the dynamics of the multipath fading channel will be driven by both the roving velocity and the motion of the receiver in the local sky:

$$\Delta\nu(t_3) \approx \Delta\nu_{\text{rover}}(t_3) + \Delta\nu_{\text{earth}}(t_3) \tag{88}$$

with

$$\Delta\nu_{\text{rover}}(t_3) \approx \frac{\vec{\boldsymbol{v}}_1 \cdot (\hat{\boldsymbol{r}}_{12} - \hat{\boldsymbol{r}}_{13})}{\lambda} \tag{89}$$

$$\Delta\nu_{\text{earth}}(t_3) \approx \frac{\vec{\boldsymbol{v}}_3 \cdot (\hat{\boldsymbol{r}}_{13} - \hat{\boldsymbol{r}}_{23})}{\lambda}. \tag{90}$$

When the vehicle is moving, the contribution to the differential Doppler shift induced by $\vec{\boldsymbol{v}}_1$ depends on the vehicle's direction of motion, which is in general arbitrary.

---

[16] In lunar applications, $|\dot{\epsilon}_0|$ is less than 0.1 deg/hour, approximately. Therefore, it is reasonable to assume that $\frac{1}{2}\dot{\epsilon}_0 T_{\text{null}} \ll \epsilon_0$ except when operating at extremely low elevation angles (i.e., when $\epsilon_0 \approx 0$). In this regime, diffraction effects beyond reflection start to be significant, so the model presented here is not entirely valid.

However, a worst case scenario, which yields maximum differential Doppler shift and thus minimum T_{null}, can be obtained using the following upper bound:

$$|\Delta\nu_{\text{rover}}(t_3)| \approx \frac{v_1}{\lambda}|\hat{\boldsymbol{v}}_1 \cdot (\hat{\boldsymbol{r}}_{12} - \hat{\boldsymbol{r}}_{13})| \leq \frac{\sqrt{2}v_{\max}}{\lambda}, \tag{91}$$

where the inequality follows from the fact that given two arbitrary unitary vectors $\hat{\boldsymbol{a}}$ and $\hat{\boldsymbol{b}}$, $|\hat{\boldsymbol{a}} - \hat{\boldsymbol{b}}|^2 = 2(1 - \hat{\boldsymbol{a}} \cdot \hat{\boldsymbol{b}}) \leq 2$. Moreover, in most circumstances we may assume that the rover antenna is directive enough so that angle between $\hat{\boldsymbol{r}}_{12}$ and $\hat{\boldsymbol{r}}_{13}$ is $\leq 90^\circ$ (in other words, the antenna does not radiate in the "backwards" direction). In that case, $\hat{\boldsymbol{r}}_{12} \cdot \hat{\boldsymbol{r}}_{13} > 0$ and, therefore,

$$|\Delta\nu_{\text{rover}}(t_3)| \leq \frac{v_{\max}}{\lambda}. \tag{92}$$

Additional expressions for $\Delta\nu_{\text{rover}}(t_3)$ require knowledge of the rover motion and the reflection geometry. For example, consider first the situation depicted in Figure 6, which generalizes Figure 5a by including the rover motion and letting the terrain be inclined by an angle α from the local zenith.[17] Using the depicted coordinate system, I observe that

$$\hat{\boldsymbol{r}}_{12} = \cos(2\alpha - \epsilon)\hat{\boldsymbol{x}} + \sin(2\alpha - \epsilon)\hat{\boldsymbol{z}} \tag{93}$$

$$\hat{\boldsymbol{r}}_{13} = \cos\epsilon\hat{\boldsymbol{x}} + \sin\epsilon\hat{\boldsymbol{z}} \tag{94}$$

$$\hat{\boldsymbol{v}}_1 = \pm\left(\cos\alpha\hat{\boldsymbol{x}} + \sin\alpha\hat{\boldsymbol{z}}\right) \tag{95}$$

which, upon using basic trigonometric identities, results in

$$\hat{\boldsymbol{v}}_1 \cdot (\hat{\boldsymbol{r}}_{12} - \hat{\boldsymbol{r}}_{13}) = 0 \tag{96}$$

for all terrain inclination angles α. Note that if $\vec{\boldsymbol{v}}_1$ has a $\hat{\boldsymbol{y}}$ component (i.e., perpendicular to the specular reflection plane), it also does not contribute to the differential Doppler shift. Therefore, we conclude that the motion of a rover in a flat possibly inclined terrain, where reflections occur in front of the vehicle, does not introduce any additional differential Doppler shift $\Delta\nu_{\text{rover}}$. In other words, the dynamics of the fading channel will be driven only by the motion of the receiver in the local sky, as would be the case for a lander.

The physical intuition behind this result is as follows: Figure 6 depicts a situation where the rover is moving in a planetary surface that is electrically flat and has infinite extent. Because the receiver is far away, the angles of the LoS and reflected rays stay constant regardless of the rover position. In other words, the rover motion simply translates the overall reflection geometry on top of the planetary surface, but it does not change the extra delay experienced by the reflected wave. Therefore, because the differential Doppler is related to the time derivative of this extra delay (see Equation (21)), I conclude that $\Delta\nu_{\text{rover}} = 0$.

---

[17] In other words, the rover's locomotion system can operate when the terrain tilt is constrained to $\leq \alpha$ degrees.

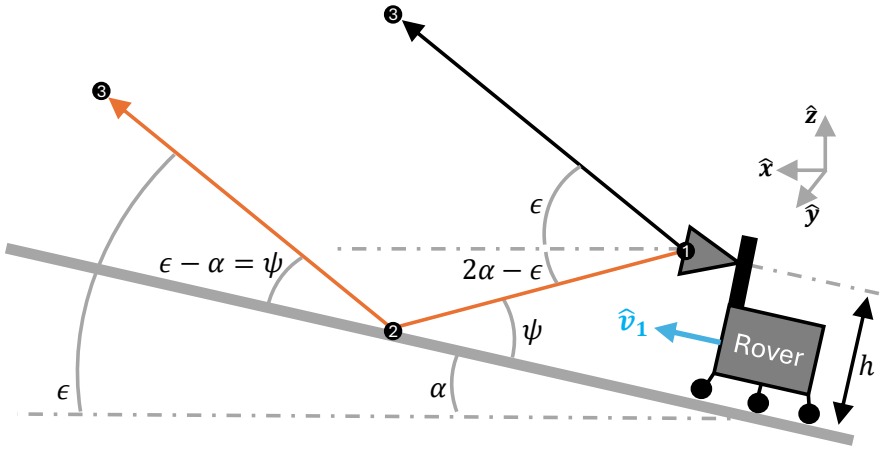

Figure 6. Reflection occurring right in front of the rover.

Next, consider the reflection geometry of Figure 7, which generalizes the system previously studied in Figure 5b. The rover velocity vector is arbitrarily oriented with respect to the reflection point, which is assumed to be at a distance and caused by a topographic feature (boulder, ridge, etc.) that is properly placed and oriented for a mostly specular reflection to occur.

Using the rover's topocentric reference frame and spherical coordinates,

$$\hat{\boldsymbol{r}}_{12} = \cos\epsilon_2 \cos\varphi_2 \hat{\boldsymbol{x}} + \cos\epsilon_2 \sin\varphi_2 \hat{\boldsymbol{y}} + \sin\epsilon_2 \hat{\boldsymbol{z}} \tag{97}$$

$$\hat{\boldsymbol{r}}_{13} = \cos\epsilon_3 \cos\varphi_3 \hat{\boldsymbol{x}} + \cos\epsilon_3 \sin\varphi_3 \hat{\boldsymbol{y}} + \sin\epsilon_3 \hat{\boldsymbol{z}} \tag{98}$$

$$\hat{\boldsymbol{v}}_1 = \cos\epsilon_v \cos\varphi_v \hat{\boldsymbol{x}} + \cos\epsilon_v \sin\varphi_v \hat{\boldsymbol{y}} + \sin\epsilon_v \hat{\boldsymbol{z}}, \tag{99}$$

where (ϵ_2, φ_2), (ϵ_3, φ_3), and (ϵ_v, φ_v) orient the location of the reflection point, the receiver, and the velocity vector in the azimuth/elevation space.[18] Therefore,

$$\hat{\boldsymbol{v}}_1 \cdot (\hat{\boldsymbol{r}}_{12} - \hat{\boldsymbol{r}}_{13}) = \cos\epsilon_v \left(\cos\epsilon_2 \cos\Delta_{v2} - \cos\epsilon_3 \cos\Delta_{v3}\right) + \sin\epsilon_v \left(\sin\epsilon_2 - \sin\epsilon_3\right) \tag{100}$$

with $\Delta_{vj} = \varphi_v - \varphi_j$, $j \in [2, 3]$. Combining this result with Equations (88) and (66) yields a final expression for the differential Doppler shift of a rover under the system geometry in Figure 7:

$$\Delta\nu(t_3) \approx \Delta\nu_{\text{rover}}(t_3) + \Delta\nu_{\text{earth}}(t_3) \tag{101}$$

with

$$\Delta\nu_{\text{rover}} = \frac{v_1}{\lambda} \left[\cos\epsilon_v \left(\cos\epsilon_2 \cos\Delta_{v2} - \cos\epsilon_3 \cos\Delta_{v3}\right) + \sin\epsilon_v \left(\sin\epsilon_2 - \sin\epsilon_3\right)\right] \tag{102}$$

$$\Delta\nu_{\text{earth}} = -\frac{r_{12}}{\lambda} \left[w_\epsilon \dot{\epsilon}_3 + w_\varphi \dot{\varphi}_3\right] \tag{103}$$

with w_ϵ and w_φ given by Equations (64) and (65).

[18] Note that (ϵ_3, φ_3) are evaluated at time t_3, whereas (ϵ_2, φ_2) and (ϵ_v, φ_v) are evaluated at time t_1.

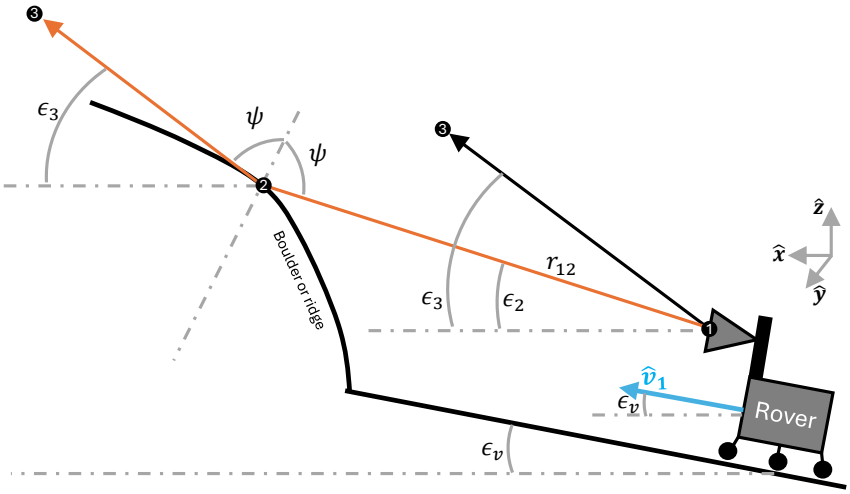

(a) Side view.

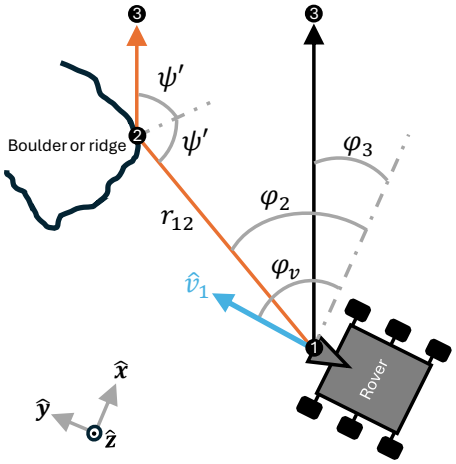

(b) Top view.

Figure 7. Illustration of a possible reflection mechanisms for a lunar rover communicating with an Earth station (not shown). Angles ψ and ψ' are arbitrary, and are shown only to emphasize that the laws of specular reflection are satisfied.

If the rover is communicating via a low gain antenna with an approximately omnidirectional radiation pattern, then the rover direction of motion is irrelevant and it is likely that the reflection point will be coaligned in azimuth with the receiver (other reflections are also possible, but ignored for simplicity). Therefore, we may assume that $\Delta_{v2} = \Delta_{v3} \equiv \Delta_v$ so that basic manipulation of Equation (100) results in

$$\Delta\nu_{\text{rover}} = \frac{v_1}{\lambda}\kappa, \tag{104}$$

where

$$\kappa = 2\sin\left(\frac{\epsilon_{23}}{2}\right)\left[\cos\epsilon_v\cos\Delta_v\sin\left(\epsilon_2 + \frac{\epsilon_{23}}{2}\right) - \sin\epsilon_v\cos\left(\epsilon_2 + \frac{\epsilon_{23}}{2}\right)\right] \tag{105}$$

with $\epsilon_{23} = \epsilon_3 - \epsilon_2$ and $\kappa \leq \sqrt{2}$ to satisfy Equation (91). Also, numerical evaluation of κ over typical ϵ_2, ϵ_3, and ϵ_v values (e.g., $\pm \sim 20$ deg, assuming a rover on the lunar south pole) results in $\kappa \leq 0.3$, approximately, thus proving a simple upper bound on the typical Doppler shift to be induced by the rover motion.

D. Null-to-Null Time Interval for a Rover

The null-to-null time interval analysis for a rover follows the same logic as for a lander (including the Taylor expansion of the receiver angular speed in the local sky), but includes the differential Doppler shift caused by the rover motion. Thus, following Equation (70), T_{null} can be computed by solving

$$\int_{t_0}^{t_0+T_{\text{null}}} \Delta\nu_{\text{rover}}(t)dt + \int_{t_0}^{t_0+T_{\text{null}}} \Delta\nu_{\text{earth}}(t)dt = 1, \tag{106}$$

For the reflection geometry depicted in Figure 6, I have concluded that $\Delta\nu_{\text{rover}}(t)$ is zero. Therefore, the derivation of T_{null} is exactly the same as for a lander, but with

$$r_{12} = \frac{h}{\sin(\epsilon - \alpha)} \tag{107}$$

$$\epsilon_{23} = 2(\epsilon - \alpha) \tag{108}$$

$$\Phi_{12} = 90^\circ. \tag{109}$$

Using the small angle approximation for operation at grazing angles leads to

$$T_{\text{null}} \approx \frac{\lambda/h}{2|\dot{\epsilon}_0|}. \tag{110}$$

which is the same result as for a lander, and does not depend on the terrain inclination angle α.

For the general case depicted in Figure 7, an analytic approximation for T_{null} is hard to obtain because:

- It depends on the roving direction, which may change during T_{null} (recall here that T_{null} can be in the order of minutes if the rover moves slowly and the reflection point is far away).
- It may be driven by phase discontinuities as the reflection point changes abruptly with the rover motion. This is most likely to occur when the reflecting terrain is close to the rover, as small changes in the vehicle position can lead to large variations in angles of incidence and reflection.

One way to overcome the first challenge is to find approximate upper and lower bounds for T_{null}. For example,

$$\int_{t_0}^{t_0+T_{\text{null}}} \Delta\nu_{\text{rover}}(t)dt \leq \int_{t_0}^{t_0+T_{\text{null}}} \frac{\sqrt{2}v_{\max}}{\lambda}dt = \frac{\sqrt{2}v_{\max}}{\lambda}T_{\text{null}}. \tag{111}$$

and, consequently,

$$\frac{\lambda}{\epsilon_0|\dot{\epsilon}_0|L+\sqrt{2}v_{\max}} \lesssim T_{\text{null}} \lesssim \frac{\lambda}{\epsilon_0|\dot{\epsilon}_0|L} \tag{112}$$

where the $\sqrt{2}$ may be replaced by 1 if the antenna only radiates in the forward direction, and the approximate upper bound is simply the null-to-null time of a lander.

Let us also consider a case where the reflection point is far away (notionally kilometers away), the terrain is mostly flat, and the rover is moving towards the point of reflection at constant speed v_1. Then, it can be assumed that

$$r_{12} = L - v_1(t-t_0) \tag{113}$$

$$\epsilon_2 \approx \epsilon_v = 0 \tag{114}$$

$$\epsilon_{23} = \epsilon \approx \dot{\epsilon}_0(t-t_0) + \epsilon_0 \tag{115}$$

$$\Phi_{12} = 90^\circ \tag{116}$$

$$\Delta_{v2} = \Delta_{v3} = 0, \tag{117}$$

which leads to

$$\int_{t_0}^{t_0+T_{\text{null}}} \left[\frac{v_1}{\lambda}(1-\cos\epsilon) - \frac{L-v_1(t-t_0)}{\lambda}\dot{\epsilon}_0 \sin\epsilon\right] dt = \frac{L}{\lambda}[\cos\epsilon_T - \cos\epsilon_0] + \frac{v_1 T_{\text{null}}}{\lambda}[1-\cos\epsilon_T] \tag{118}$$

with $\epsilon_T = \epsilon_0 + \dot{\epsilon_0} T_{\text{null}}$. Next, we need to simplify this equation to yield a closed-form solution for T_{null}. One option is to assume that $\dot{\epsilon_0} T_{\text{null}} \approx 0$, i.e., solve the problem ignoring the motion of Earth in the local sky. In that case, the first terms in the right-hand side of Equation (118) is zero and, consequently,

$$T_{\text{null}} \frac{v_1}{\lambda}(1-\cos\epsilon_0) = 1, \tag{119}$$

which yields

$$T_{\text{null}} \approx \frac{\lambda}{v_1(1-\cos\epsilon_0)}. \tag{120}$$

This result is expected, it simply states that $T_{\text{null}} \approx \frac{1}{\Delta\nu_{\text{rover}}}$. In other words, the time required for the channel to experience two consecutive fades is equal to the time it takes for the rover to move enough distance so that the differential phase has advanced by one cycle (i.e., by λ meters).

To obtain an approximate estimate of T_{null} that includes the motion of Earth we note that

$$\cos\epsilon_T - \cos\epsilon_0 = -2\sin\left(\epsilon_0 + \frac{\dot{\epsilon_0} T_{\text{null}}}{2}\right)\sin\frac{\dot{\epsilon_0} T_{\text{null}}}{2} \approx -\dot{\epsilon_0} T_{\text{null}} \sin\epsilon_0 \tag{121}$$

where the second equality follows from assuming that $\epsilon_0 \gg \dot{\epsilon_0} T_{\text{null}}$ and $\dot{\epsilon_0} T_{\text{null}} \approx 0$ so that the small angle approximation for the sine can be invoked. Therefore, T_{null} is found by solving

$$-\frac{L}{\lambda}\dot{\epsilon_0} T_{\text{null}} \sin\epsilon_0 + T_{\text{null}} \frac{v_1}{\lambda}(1-\cos\epsilon_0) = 1 \tag{122}$$

which results in

$$T_{\text{null}} \approx \frac{\lambda}{v_1(1-\cos\epsilon_0) - L\dot{\epsilon_0}\sin\epsilon_0}. \tag{123}$$

Note that this result is a combination of two terms: The contribution to T_{null} from the rover motion, as captured by $\frac{1}{\Delta\nu_{\text{rover}}}$, and the contribution from the Earth motion, as captured by Equation (87), and with the signs dictated by the direction of motion of the vehicle and whether Earth is rising or setting in the local sky.

IV. Dynamics of an Uplink with a Single Coherent Reflection

If we assume that the surface of the planetary body causing the reflection behaves as a time-invariant linear electromagnetic medium, as is commonly the case for the Moon or Mars, then Maxwell's equations dictate that the resulting multipath fading channels must be reciprocal [8]. In other words, at any point in time a propagation path from transmitter to receiver carries the same amount of power in both the uplink and downlink direction, regardless of whether than path experiences a reflection or not. Therefore, even though the model of Section II was derived under the assumption of downlink transmission, its results are also applicable for the uplink direction. This is particularly evident when considering the derived formula for the differential Doppler shift (see Equation (40)), which is the basis for estimating the null-to-null interval. It states that $\Delta\nu(t)$ is equal to difference traveled by the LoS and reflected rays, with distance being a physical quantity that does not have associated directionality. Therefore, we conclude that the values of T_{null} expected on the uplink and downlink directions are equal.

V. Results

This section is divided in two parts. First, I describe the geometry of a DTE link for two operational tracks executed between an Earth station and a lander close to the lunar South Pole.[19] Then, I analyze the recorded signal to determine the null-to-null time interval and I compare it against predictions generated from the analytical model presented in the previous section.

I consider two DTE links for the analysis. The first link occurred on the 2024th day of year 235, between the CH3 lander and deep space station (DSS) 65 in the Madrid Deep Space Communication Complex (MDSCC). Approximately 5 hours of surface operations were supported by the DSN, all exhibiting clear multipath effects. A second set of surface operations exhibiting multipath reflections occurred during the IM1 mission, which landed on the Moon on 02/22/2024. DSN provided extensive emergency support due to the off-nominal lander orientation, using both DSS-24 at

[19] Because no empirical data is available from a rover on the lunar South Pole, this section focuses exclusively on analyzing reflections from two landers.

the Goldstone Deep Space Communication Complex (GDSCC) and DSS-36 at the Canberra Deep Space Communication Complex (CDSCC).

A. DSN Support for CH3

CH3 landed in the Siv Shakti Point on 08/23/2023, at 12:33 UTC. Its final landing location was 69.373° S, 32.319° E, 529.2m, approximately 632 km away from the lunar South Pole (see Figure 8a), in a relatively flat area with a ridge situated ∼6.4 km away and properly aligned to cause a strong coherent reflection towards Earth (see Figure 8b). During landing, Earth was approximately 11° above the lunar local terrain, and it dipped down to 6° or 7° at its lowest point, later in the mission (see Figure 8c).

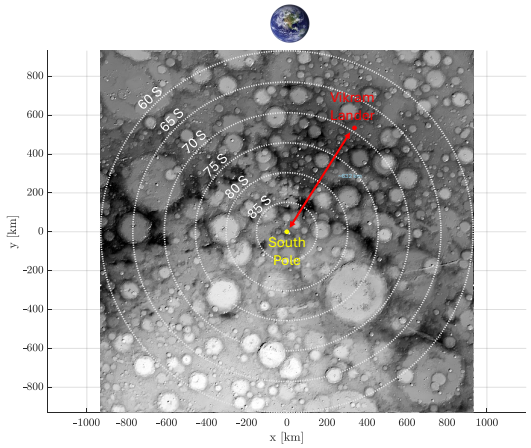

(a) Stereographic projection of the lunar South Pole with the landing location of the Vikram Lander.

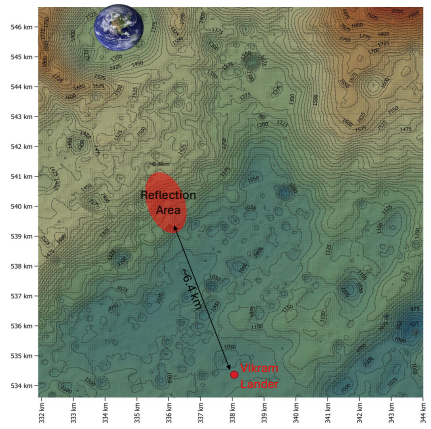

(b) Map showing the topography around the Vikram Lander and identifying the reflection point, in a ridge 6.4 km away in the Earth direction.

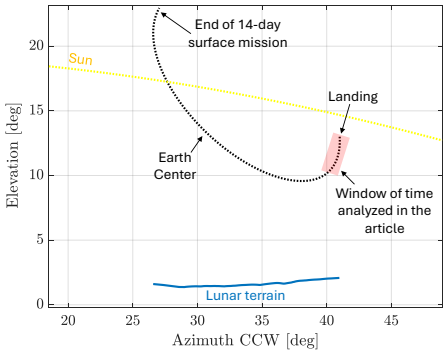

(c) Elevation of Earth in the local lunar sky, as seen by the Vikram Lander during its surface operations. The lunar terrain mask is calculated using digital elevation maps of the Moon.

Figure 8. Landing geometry for the Vikram Lander, part of the Chandrayaan-3 mission.

DSN provided tracking support to CH3 for several days prior to landing, as well

during its powered descent and for the first 8 hours of landed operations. However, to analyze multipath effects, I consider only the support provided from 16:18 UTC to 20:18 UTC, which provides several hours of clean data to study the null-to-null time interval. In that sense, Figure 9 shows a timeline of received carrier power to spectral noise density (P_c/N_0) at DSS-65 (S-band, 2.24 GHz), approximately 3 hours after landing. P_c/N_0 estimates were generated by the DSN receivers and stored at a cadence of 1 observation every 5 seconds, approximately. The resulting time series can be decomposed into three components:

- The long-term trend of received power, shown with an orange dotted line, is estimated using a 1-hour moving average. It is attributed to causes other than multipath such as variations in the transmit antenna gain as Earth moves in the lunar sky and increased atmospheric effects due to operation at low elevation angles on Earth.
- The received power, including a single coherent reflection, is shown in yellow and was calculated using a 20-seconds moving average. This value has been adjusted to ensure that the fading cadence on the order of a few minutes is clearly observable, but shorter term oscillations are averaged out.
- The received power, including coherent and non-coherent reflections, is shown in blue, using the original 5-second time series. It includes short term power variations attributable to non-coherent reflections from the rough lunar surface, superimposed on the coherent and long-term trends.

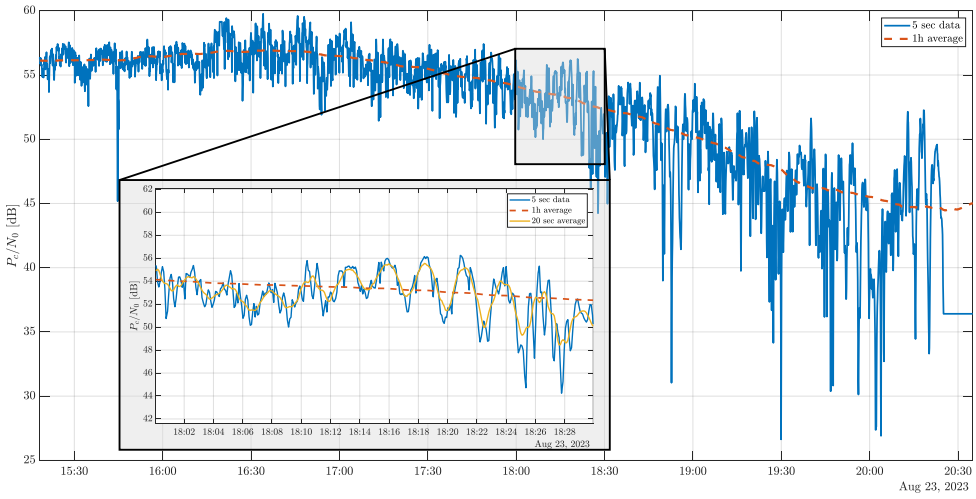

Figure 9. Received P_c/N_0 as a function of time during the CH3 surface operations.

Adjusting the averaging time to recover the coherent component of the reflection is ultimately a judgment call by the analyst and, if not done correctly, can bias the measurement of T_{null}. Therefore, in this article I have first estimated the power spectral density (PSD) of the received P_c/N_0 time series, after demeaning, and noted

that it exhibits a clear peak at 0.02 Hz, approximately (see Figure 10). This indicates that the time series has oscillations occurring at a cadence of 50 seconds or a minute, so averaging for periods longer than this value will most likely average out the coherent component. Therefore, a value of 20 seconds is selected.

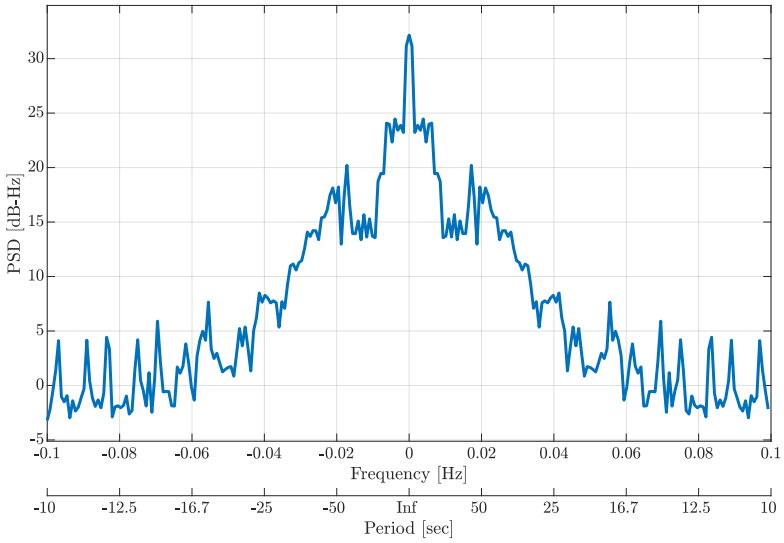

Figure 10. PSD of the CH3 P_c/N_0 time series, after demeaning.

Once the coherent part of the reflection has been recovered, T_{null} can be directly inferred by searching the moments in time where the received P_c/N_0 is minimized. Numerically, this can be accomplished using an algorithm to find local maxima in an arbitrary function, such as the one documented in Matlab's "findpeaks" function [6]. This leads to the results shown in Figure 11, where red dots are used to mark the moments of deep fade detected by the algorithm. Note that this approach produces some false positives starting at 19:15 UTC and until the end of the time series. This is due to the fact that, during this time period, the measured reflection is significantly more non-coherent, thus causing faster than expected fades of unpredictable depth, which makes it more difficult to detect the moments when a coherent null occurred.

Finally, I can now compare the T_{null} values derived from Equation (87) against the estimates obtained from the empirical data. In particular, I let $L = 6.4$ km based on Figure 8b and use SPICE to calculate values for ϵ_0 and $|\dot{\epsilon}_0|$ assuming CH3 was tracked by DSS-65 during the analysis period. The results are shown in Figure 12, where the empirical data is shown in black, and the approximated analytical expression is shown in orange. It can be observed that there is good agreement between the empirical data and the model until 19:00 or 19:30 UTC, with the average null-to-null time interval closely matching the value predicted by the model. Starting at 19:00 UTC, we see that the model breaks down, mostly induced by the non-coherent reflections and their resulting power oscillations. However, visual inspection of the last 30 minutes of the P_c/N_0 time series shows that most of the large fades do occur at a cadence of 4 to 5

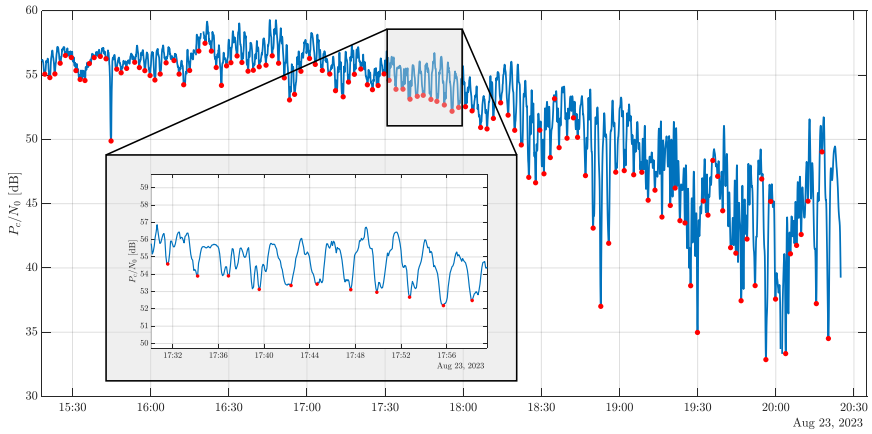

Figure 11. Detection of moments of deep fade using Matlab's "findpeaks" algorithm.

minutes approximately, which is consistent with the upward trend in the orange plot of Figure 12.

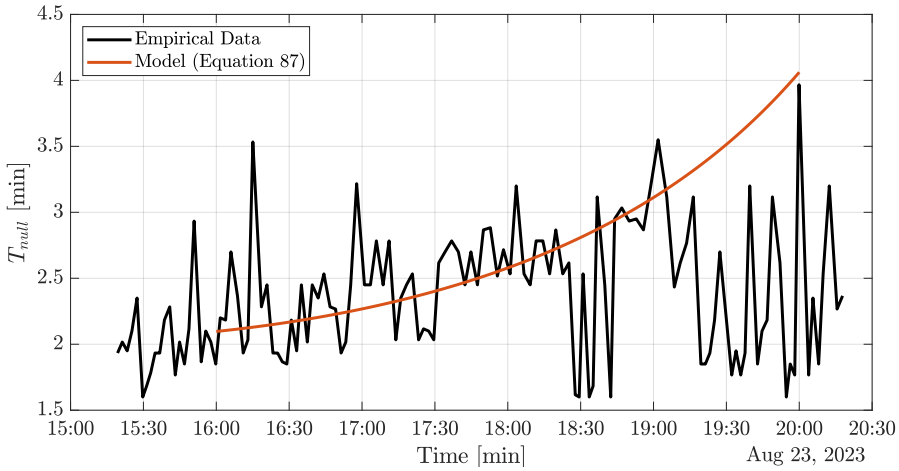

Figure 12. Comparison of T_{null} values for the surface of operations of the CH3 lander.

B. DSN Support for IM1

The same analysis was performed for a track executed on 2024, day-of-year 57, between the IM1 lander and DSS-36. Similar to CH3, this track was selected because it provided several opportunities to measure deep fades, thus providing numerous data points for T_{null} comparison.

IM1 landed at 80.1276° S, 1.4367° E, in an area close to the top of Mount Malapert. Because of the off-nominal landing sequence, the final resting place was ∼3 km away from the expected landing location, in a sloped area that provided the necessary

conditions for a strong coherent reflection to occur two kilometers away from the lander (see Figure 13). During surface operations, only the vehicle's low gain antennas were oriented properly for communicating with Earth. Therefore, the DTE link was established at S-band (2210.6 MHz), and experienced low elevation angles ranging from 15 deg at landing down to 10 deg during the last contact. Furthermore, the null-to-null cadence was driven by the motion of DSS-36 in elevation on the lunar sky, which varied at a rate of 0.12 deg per hour, approximately.

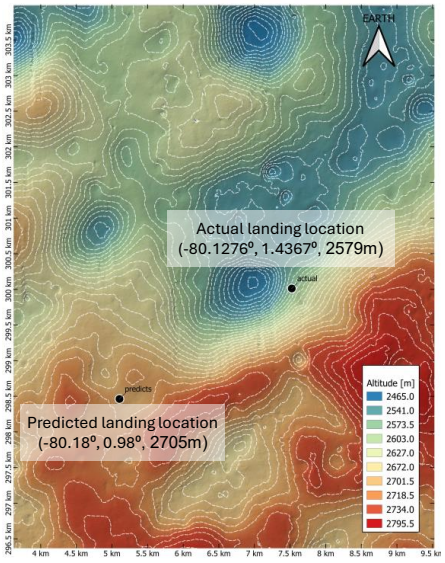

(a) Mount Malapert region around the IM1 landing location.

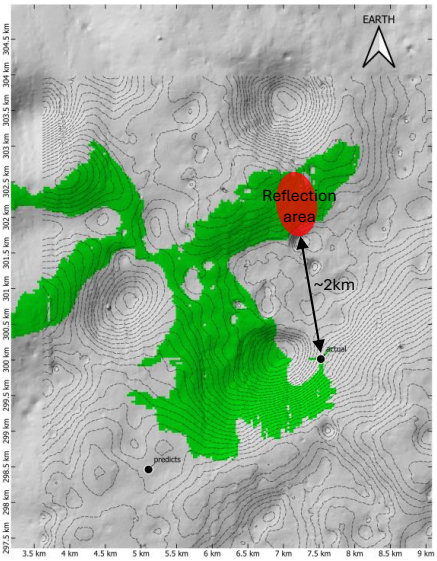

(b) Viewshed analysis of the IM1 landing location. Green areas indicate line-of-sight from the lander. The red area notionally depicts the position of the coherent reflection point.

Figure 13. Landing geometry for the Vikram Lander, part of the Chandrayaan-3 mission.

Using open loop recordings from DSS-36, we reconstructed estimates of signal power over noise spectral density (P_s/N_0) for the IM1 lander. This information was then post-processed to extract the coherent and non-coherent reflection components and derive instants of time with deep fades, in a manner akin to the CH3 lander. The result of this process is shown in Figure 14, which plots the received P_s/N_0 with red dots indicating moments of deep fades. As with CH3, the algorithm to detect deep fades generates some false positives (e.g., around 13:30 UTC), but for the most part it correctly identifies the moments where the reflection was out of phase with the line-of-sight ray.

The comparison of T_{null} between the empirical data and the model from Equation (87) is shown in Figure 15. Once again, we observe that the predicted null-to-null cadence matches well with the measured value, to within a couple of minutes, increasing confidence in the presented model and our ability to predict the cadence of nulls prior to launch and/or landing of future lunar missions.

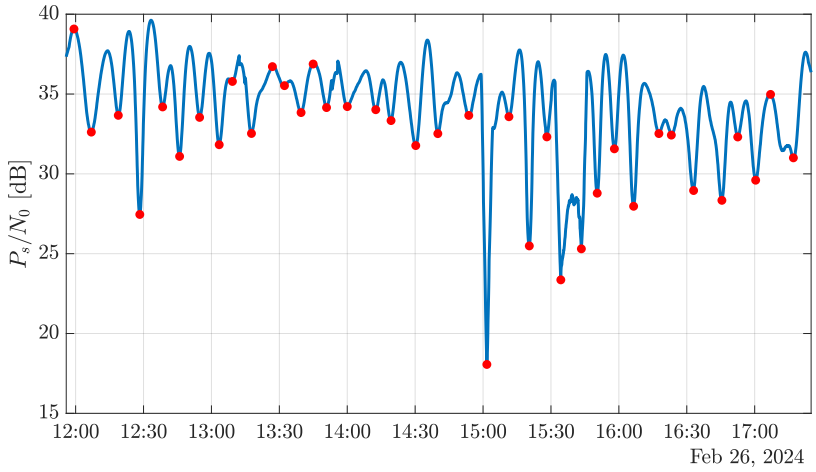

Figure 14. Comparison of T_{null} values for the surface of operations of the IM1 lander.

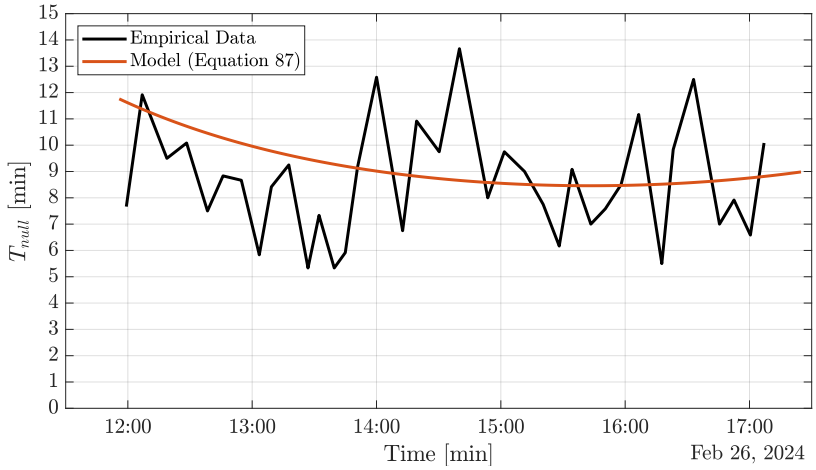

Figure 15. Comparison of T_{null} values for the surface of operations of the IM1 lander.

VI. Conclusions

This article contains three contributions: First, it provides a comprehensive model of a coherent reflection from a spacecraft near or one the surface of a planetary body and, through a series of approximations, derives simplified expressions for the differential delay and differential Doppler shift. It shows that for a lander, the differential Doppler shift, which drives the dynamics of the multipath channel, is a function of the angular velocity of the receiver in the local sky of the planetary body, while a rover experiences an additional contribution from the rover velocity that accelerates the null-to-null cadence.

The second contribution is to describe the first ever empirical measurements of multipath effects experienced by vehicles landed on the lunar South Pole. Two 5 hour tracks are presented, one for the CH3 spacecraft, and another one for the IM1 mission.

In both cases, it is shown that the geometry of the landing site was such that, at integration times of ∼1 second, the multipath phenomenon can be modeled as a single reflection towards Earth, causing periodic oscillations in the received power with a cadence directly proportional to the distance between the lander and the point of reflection.

Finally, the third contribution is to compare the null-to-null time interval as measured from the empirical data vs. the value estimated with the model presented in this article. We show that for the two geometries studied, the model agrees well with the measured data when the reflection is mostly coherent, successfully explaining why IM1 experienced a multipath channel that was significantly slower than CH3.

A. Future Work

Several avenues of future work are possible. From an empirical standpoint, additional data collected in DTE links between future lunar missions and the DSN will help further solidify the results presented in this paper, especially if they correspond to reflection geometries different from the ones already studied herein.

From a technological standpoint, the results of this paper suggest that several mitigation techniques could be used to improve resilience of DTE links against multipath. For example, smart automatic repeat request (ARQ) schemes in which the transmitter autonomously adjusts the retransmission timers based on real-time estimates of T_{null} could be used to reclaim several dBs in the link budget. Similar gains may also be achievable using rake receiver structures that estimate and subtract the reflection, assuming the symbol rate is high enough to estimate its delay reliably, or by using a rake receiver or an equalizer together with a spread spectrum sequence that is suitable for estimating the channel impulse response at the receiver.

Acknowledgments

The research was carried out at the Jet Propulsion Laboratory, California Institute of Technology, under a contract with the National Aeronautics and Space Administration (80NM0018D0004).

The author would like to acknowledge Kar-Ming Cheung of the JPL for his comments and support of this work. The author would also like to acknowledge Pater Basch of the JPL for the thorough editorial review.

References

[1] Marc Sanchez Net. Simulation of Multipath Reflections from Planetary Bodies: Theory and Application to the Lunar South Pole. The Interplanetary Network Progress Report, Volume 42-226, pp. 1-53, August 15, 2021.

https://ipnpr.jpl.nasa.gov/progress_report/42-226/42-226D.pdf

[2] L. Tadjpour and D. Bell, "Multipath Mitigation on In Situ Communication Links," The Interplanetary Network Progress Report, Volume 42-151, pp. 1-21, November 15, 2002. https://ipnpr.jpl.nasa.gov/progress_report/42-151/151F.pdf

[3] Vogel, Wolfhard J., and Julius Goldhirsh. "Multipath fading at L band for low elevation angle, land mobile satellite scenarios." IEEE Journal on Selected Areas in Communications 13, no. 2 (1995): 197-204.

[4] Haynes, Mark S. "Surface and subsurface radar equations for radar sounders." Annals of Glaciology 61, no. 81 (2020): 135-142.

[5] Willis, Nicholas J. Bistatic radar. Vol. 2. SciTech Publishing, 2005.

[6] Mathworks, 2024. https://www.mathworks.com/help/signal/ref/findpeaks.html

[7] "Deep Space Network Services Catalog," Jet Propulsion Laboratory, Technical Report 820-100, Rev. H, June 2022. https://deepspace.jpl.nasa.gov/files/820-100-H.pdf

[8] Jakes, William C. Microwave Mobile Communications. Wiley-Interscience, 1974.